JGR Atmospheres

RESEARCH ARTICLE
10.1029/2022JD037700

Were Wildfires Responsible for the Unusually High Surface Ozone in Colorado During 2021?

Andrew O. Langford[1], Christoph J. Senff[1,2], Raul J. Alvarez II[1], Ken C. Aikin[1,2], Ravan Ahmadov[2,3], Wayne M. Angevine[1,2], Sunil Baidar[1,2], W. Alan Brewer[1], Steven S. Brown[1,4], Eric P. James[2,3], Brandi J. McCarty[1,2], Scott P. Sandberg[1], and Michael L. Zucker[1,2]

[1]NOAA Chemical Sciences Laboratory, Boulder, CO, USA, [2]Cooperative Institute for Research in Environmental Sciences, University of Colorado, Boulder, CO, USA, [3]NOAA Global Systems Laboratory, Boulder, CO, USA, [4]Department of Chemistry, University of Colorado, Boulder, CO, USA

Abstract Ground-level ozone (O_3) was unusually high in northern Colorado in the summer of 2021 with maximum daily 8-hr average (MDA8) concentrations 6 to 8 parts-per-billion by volume (ppbv) higher than in 2019, 2020, or 2022. One or more of the monitors on the Colorado Front Range exceeded the 2015 U.S. National Ambient Air Quality Standard (NAAQS) of 70 ppbv on 66 of the 122 days from 1 June to 30 September, and this record number of exceedances coincided with the near daily presence of dispersed smoke haze from wildfires in Arizona, California, and the Pacific Northwest. In this paper, we use regulatory and non-regulatory surface O_3 and $PM_{2.5}$ measurements in conjunction with ground-based lidar observations to estimate how much O_3 was associated with the wildfire smoke. Analyses of the surface measurements suggest that pyrogenic O_3 transported to northern Colorado with the smoke increased the surface concentrations in northern Colorado by an average of 8 ppbv in July, 3 ppbv in August, and 2 ppbv in September. Analysis of the lidar measurements showed these contributions to be as large as 12 ppbv on some days. Production of O_3 from reactions of pyrogenic VOCs and locally emitted NO_x appears to have been minimal (<3 ppbv) in the Boulder area, but may have been much larger in the suburbs southwest of downtown Denver.

Plain Language Summary Northern Colorado experienced unusually poor air quality in the summer of 2021 with frequent high ozone (O_3) episodes and hazy skies caused by smoke from wildfires in Arizona, California, and the Pacific Northwest. In this study, we use surface and lidar measurements to explore the connection between the two. Our analysis suggests that the unusually high O_3 was caused primarily by a combination of O_3 transported to Colorado with the wildfire smoke and enhancement of local photochemical production by unusually clear skies and warm temperatures coupled with weak winds that led to localized O_3 accumulations and fewer than normal thunderstorms that might otherwise have dispersed the O_3. Production of O_3 by reactions of locally emitted NO_x with VOCs in the wildfire smoke may also have been significant in Southwest Denver.

Key Points:

- The impacts of the 2021 western wildfires on ozone in the Denver metropolitan area and rural northern Colorado in 2021 are examined
- Ozone transported in the smoke from distant wildfires increased the 8-hr concentrations in northern Colorado by an average of 8 ppbv in July
- Unusual meteorology, including fewer thunderstorms, allowed ozone produced locally to accumulate along the foothills west of Denver

Supporting Information:

Supporting Information may be found in the online version of this article.

Correspondence to:

A. O. Langford,
andrew.o.langford@noaa.gov

Citation:

Langford, A. O., Senff, C. J., Alvarez, R. J. II, Aikin, K. C., Ahmadov, R., Angevine, W. M., et al. (2023). Were wildfires responsible for the unusually high surface ozone in Colorado during 2021? *Journal of Geophysical Research: Atmospheres*, *128*, e2022JD037700. https://doi.org/10.1029/2022JD037700

Received 22 AUG 2022
Accepted 22 MAY 2023

Author Contributions:

Conceptualization: Andrew O. Langford, Steven S. Brown
Data curation: Christoph J. Senff, Raul J. Alvarez II
Formal analysis: Andrew O. Langford, Sunil Baidar

1. Introduction

The adverse impacts of wildfires on ambient air quality and human health have grown in recent years as climactic shifts and long-standing fire suppression practices have increased fire activity across the western U.S. and Canada (Bryant & Westerling, 2014; Westerling et al., 2016). Wildfires generate large quantities of carbon monoxide (CO) and carbon dioxide (CO_2) in addition to primary and secondary fine particulates ($PM_{2.5}$), and also produce a variety of other gaseous compounds including the reactive nitrogen oxides ($NO + NO_2 = NO_x$) and volatile organic compounds (VOCs) that are the photochemical precursors of ozone (O_3). The negative health effects of CO, O_3, NO_2, and $PM_{2.5}$ have long been recognized, and these pollutants comprise four of the six "criteria" air pollutants regulated by the U.S. Clean Air Act (CAA) and are subject to National Ambient Air Quality Standards (NAAQS) (Karstadt et al., 1993). Ozone and $PM_{2.5}$ both impair lung and cardiovascular function (Brown et al., 2008; Reid et al., 2016) and recent studies (Kalashnikov et al., 2022) suggest that exposure to wildfire smoke containing both O_3 and $PM_{2.5}$ can have more severe health impacts than exposure to either pollutant alone.

The production of O_3 by wildfires depends on many factors (Jaffe et al., 2018; Jaffe & Wigder, 2012) that affect the NO_x and VOC precursor emissions (e.g., fuel type and moisture content), the photochemical reaction rates (e.g., plume height and density), or both (e.g., meteorology) (Xu et al., 2021). Ozone concentrations

Investigation: Andrew O. Langford, Raul J. Alvarez II, Ken C. Aikin, Wayne M. Angevine, Sunil Baidar, Steven S. Brown, Scott P. Sandberg
Methodology: Andrew O. Langford, Christoph J. Senff
Resources: Raul J. Alvarez II, Ravan Ahmadov, W. Alan Brewer, Steven S. Brown, Eric P. James, Brandi J. McCarty, Scott P. Sandberg, Michael L. Zucker
Software: Ken C. Aikin
Supervision: W. Alan Brewer, Steven S. Brown
Validation: Andrew O. Langford, Christoph J. Senff, Brandi J. McCarty
Visualization: Andrew O. Langford, Ken C. Aikin, Ravan Ahmadov, Steven S. Brown
Writing – original draft: Andrew O. Langford
Writing – review & editing: Andrew O. Langford, Christoph J. Senff, Wayne M. Angevine, Sunil Baidar, Steven S. Brown

often decrease in the immediate vicinity of a fire when ambient O_3 reacts with freshly emitted NO (Alvarado et al., 2010), but increase downwind as the fresh NO is oxidized to NO_2 and the NO_x-VOC photochemical cycle becomes established. Ozone production falls off after a few hours for emissions during the most active part of the fire cycle in mid-afternoon (Calahorrano et al., 2021; Robinson et al., 2021) as the NO_x is converted into more stable compounds like peroxyacyl nitrates (PANs) and nitric acid (HNO_3), but moderate O_3 production can be sustained over hundreds or even thousands of kilometers downwind as PAN decomposes (Bourgeois et al., 2021; McKeen et al., 2002; Wotawa & Trainer, 2000). Even NO_x-depleted wildfire smoke can increase O_3 in urban areas, however, if the residual pyrogenic VOCs (PVOCs) mingle with NO_x from transportation sources, energy production, and other human activities (Ninneman & Jaffe, 2021; Singh et al., 2012). The ability to differentiate between this O_3 and that formed upwind in the nascent smoke plume has important implications for the design of O_3 mitigation strategies.

Both 2020 and 2021 were severe wildfire years across much of the western U.S. with new records set for the number of acres burned in both Colorado and California in 2020 (see Supporting Information S1). The Colorado Department of Public Health and Environment (CDPHE) issued 43 "Ozone Action Day Alerts" for the Denver Metro/Northern Front Range (DM/NFR, Figure 1) during the 2020 "ozone season" lasting from 31 May to 31 August, and 65 ozone action day alerts for the DM/NFR in 2021. For comparison, only 32 and 40 alerts were issued in 2019 and 2022, respectively, which were low wildfire years. These differences suggest that wildfires contributed to the higher O_3 in both 2020 and 2021, but quantifying the net contribution in 2020 is complicated by the mingling of fresh smoke plumes from the nearby Colorado wildfires with the aged smoke haze from distant wildfires in California and the Pacific Northwest (PNW) (Rickly et al., 2023). There were relatively few wildfires in Colorado during 2021, however, which allows us to estimate the influence of the dispersed smoke haze from the out of state wildfires by comparing surface O_3 and $PM_{2.5}$ measurements (Section 4) from the DM/NFR with those from the more sparsely populated Western Slope (WSLP). We then use ground-based lidar measurements from Boulder (Section 5) to examine the entrainment of pyrogenic O_3 on individual days.

2. Background

Ground level O_3 declined across most of the United States over the last 20 years (Figure 2a) as improved controls have reduced NO_x emissions from the energy and transportation sectors (Gaudel et al., 2018). The average of the fourth highest MDA8 O_3 concentration (4MDA8), the metric used by the EPA to determine compliance with the NAAQS, measured by 842 regulatory monitors decreased by ≈20% between 2000 and 2021 (https://www.epa.gov/air-trends/ozone-trends). The largest changes were in the Southeast, where the mean 4MDA8 decreased by ≈25%, but the mean 4MDA8 declined by only 2% in the Southwest including Colorado, and remained flat in the Denver metropolitan area despite a more than 70% decrease in the mean summertime NO_2 concentrations over the same period (Figure 2b). The 10%–15% dip in mean NO_2 between 2019 and 2020 likely reflects the effects of the COVID-19 slowdown. The DM/NFR encompasses the Wattenberg Gas Field of the Denver-Julesburg Basin and recent studies suggest that some parts of the DM/NFR are now in a NO_x-sensitive O_3 production regime during the summer (McDuffie et al., 2016; Pollack et al., 2021).

Measurements downloaded from the U.S. EPA Air Quality System (AQS) (US EPA, 2023a) show that the maximum daily 8-hr (MDA8) O_3 concentrations at one or more of the 16 monitors in the DM/NFR non-attainment area (Figure 1) were in exceedance of the 2008 NAAQS of 75 parts-per-billion by volume (ppbv) on 47 days, and the more stringent 2015 O_3 NAAQS of 70 ppbv on 66 days between 1 June and 30 September 2021. A means of quantifying the contributions of wildfires and other non-controllable sources to these high concentrations is critically needed since the current (2019–2021) DM/NFR design value, that is, the 3-year average of the fourth highest annual MDA8 concentration and the metric used by the EPA use to determine compliance with the NAAQS, is 83 ppbv or the highest of any area outside the state of California (US EPA, 2023b). The DM/NFR was recently reclassified from "serious" to "severe" non-attainment of the 2008 NAAQS (US EPA, 2022c) and from "marginal" to "moderate" non-attainment of the 2015 NAAQS (US EPA 2022a). The paradoxically lower designation for the more stringent 2015 NAAQS reflects the longer timeline for full implementation of the new standard, which will be in 2038 for the most severely polluted areas (US EPA 2022b).

Figure 2a shows that the 4MDA8 O_3 in the Denver area jumped from 72 ppbv in 2019, which was a low wildfire year, to 82 ppbv in 2020 and 84 ppbv in 2021. The corresponding 4MDA8 O_3 concentrations at the Chatfield State Park monitor were 78, 83, and 89 ppbv, respectively. This suburban monitor is located near the foothills

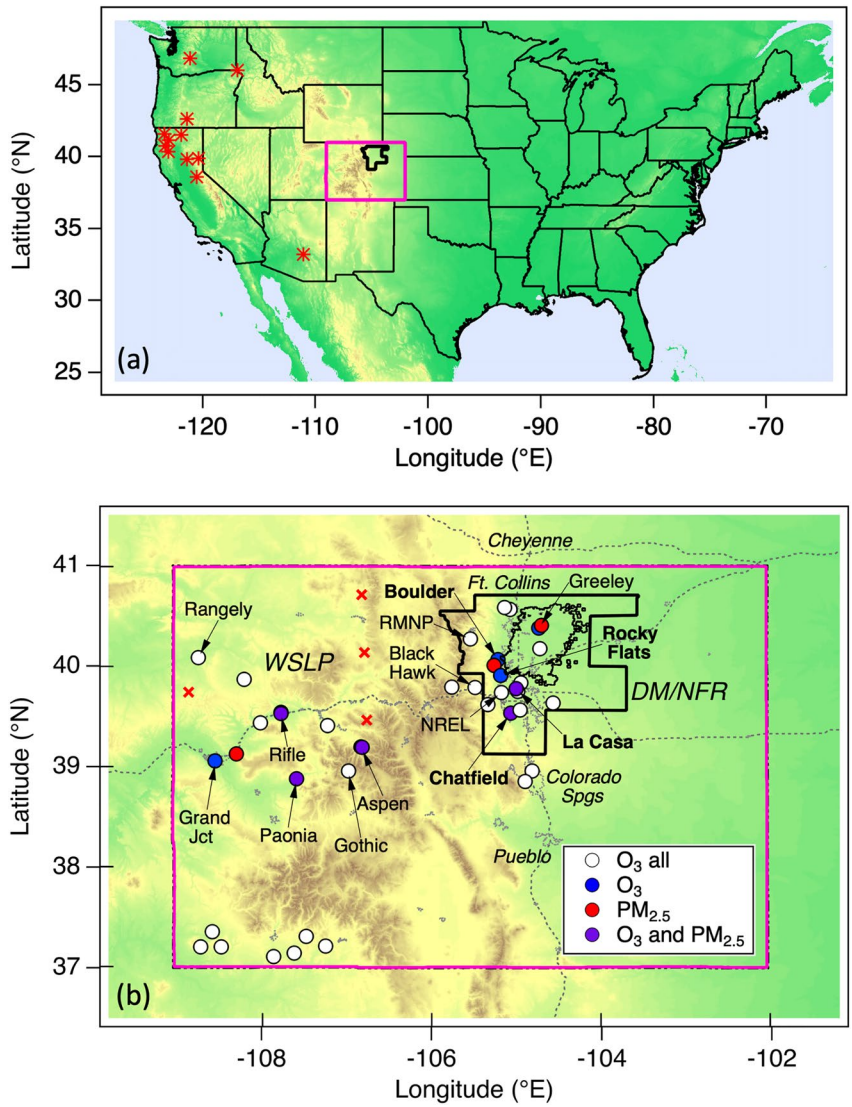

Figure 1. (a) Relief map of the U.S. showing the state of Colorado and the Denver Metro/North Front Range (DM/NFR) non-attainment area. The red asterisks mark the locations of the 2021 megafires. (b) Enlarged view of Colorado showing the locations of the DM/NFR and Western Slope (WSLP) O_3 and $PM_{2.5}$ monitors used in the analysis (blue, red, and purple filled circles). Much of the discussion focuses on the Paonia (PAOA), Chatfield State Park (CHAT), Rocky Flats-North (RFN), and Boulder (BOU) monitors. The white filled circles show additional O_3 monitors operated by the CDPHE, USNPS, EPA, and Southern Ute tribe. The DM/NFR includes most of the Front Range Urban Corridor, which extends from Pueblo, CO in the south to Cheyenne, WY to the north, as well as the Wattenberg Gas Field of the Denver-Julesburg Basin (irregular black outline). The red crosses mark the locations of the four largest Colorado wildfires during the June-September measurement period (see Table S1 in Supporting Information S1).

about 25 km southwest of downtown Denver (cf. Figure 1b) and routinely measures the highest O_3 in the DM/NFR (see below). National statistics for 2022 were not yet available at the time of writing, but the 4MDA8 at the Chatfield monitor returned to 78 ppbv in 2022. Figure 2c shows that the 24-hr $PM_{2.5}$ at the two main Denver monitoring stations also increased in 2020 and 2021 due to the frequent presence of wildfire smoke (see Figure S1 in Supporting Information S1). Although 2020 was a record-breaking wildfire year in Colorado, two of the three megafires (i.e., >100,000 ac) that burned near the Front Range urban corridor started in mid-September and October and their contributions to the June-September averages are relatively minor.

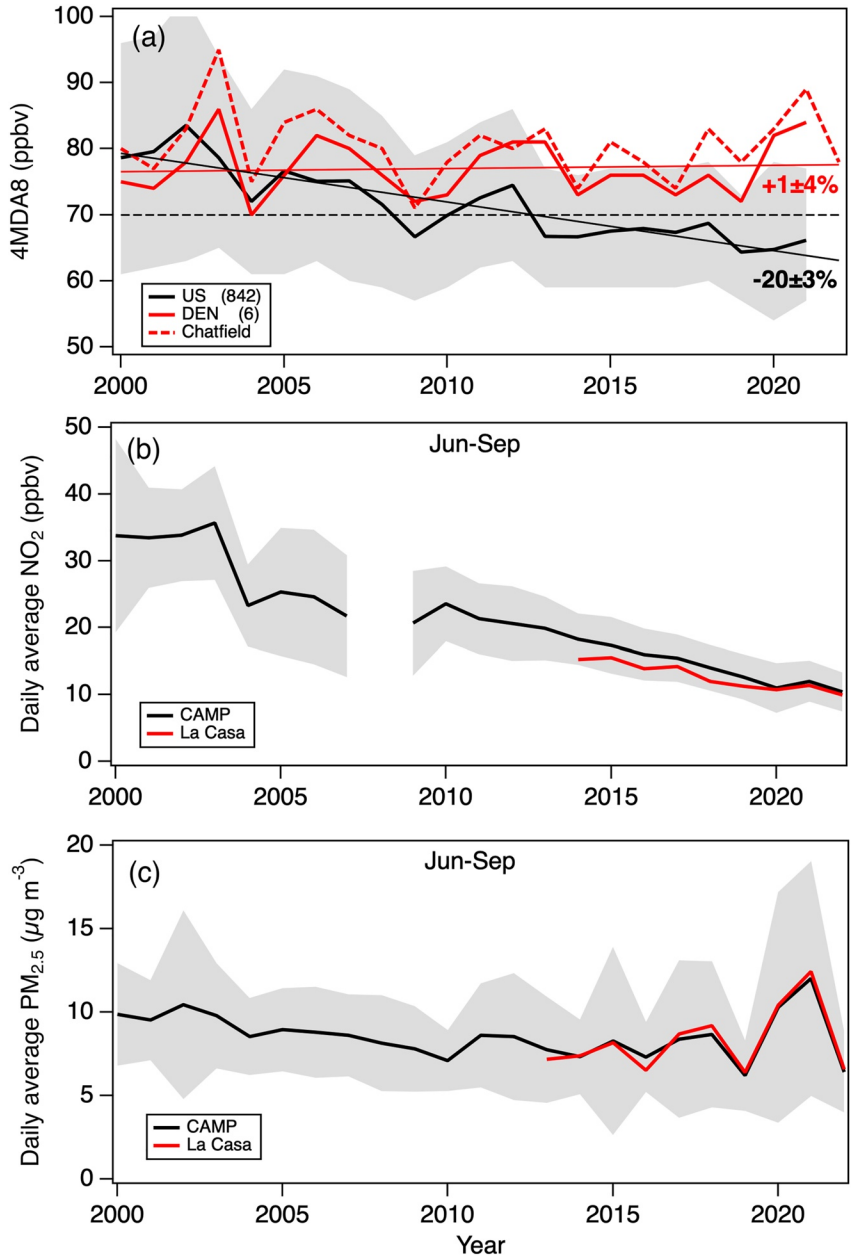

Figure 2. (a) Spatially averaged annual fourth highest MDA8 O_3 measured between 2000 and 2021. Measurements are shown for the entire U.S. (842 monitors), and the Denver-Aurora-Lakewood MSA (six monitors). The net changes corresponding to the linear regression fits (solid lines) are shown. The measurements from the Chatfield (CHAT) monitor are also plotted. The 2015 NAAQS is represented by the black dashed line. The gray shading shows the 10th and 90th percentiles. (b) Daily mean NO_2 and (c) daily mean $PM_{2.5}$ concentrations (June-September averages) from the CAM and La Casa monitors in Denver. The gray shading shows the standard deviations of the averages. Source: https://www.epa.gov/air-trends.

3. Meteorological Context

Unusual meteorological factors may also have favored the production and accumulation of O_3 in the Denver-Boulder metropolitan area in 2021. Photochemical production of O_3 is enhanced by clear skies and warm temperatures (Sillman & Samson, 1995) and the 500 hPa geopotential height and 850 hPa temperature anomaly plots from the NCAR/NCEP (National Center for Atmospheric Research/National Center for Environmental Prediction) Reanalysis in Figure 3 show that both were elevated above the PNW and Intermountain West (IMW) during the summers (1 June to 30 September) of 2021 and 2022 compared to the 2019 and 2020 and to the 30-year

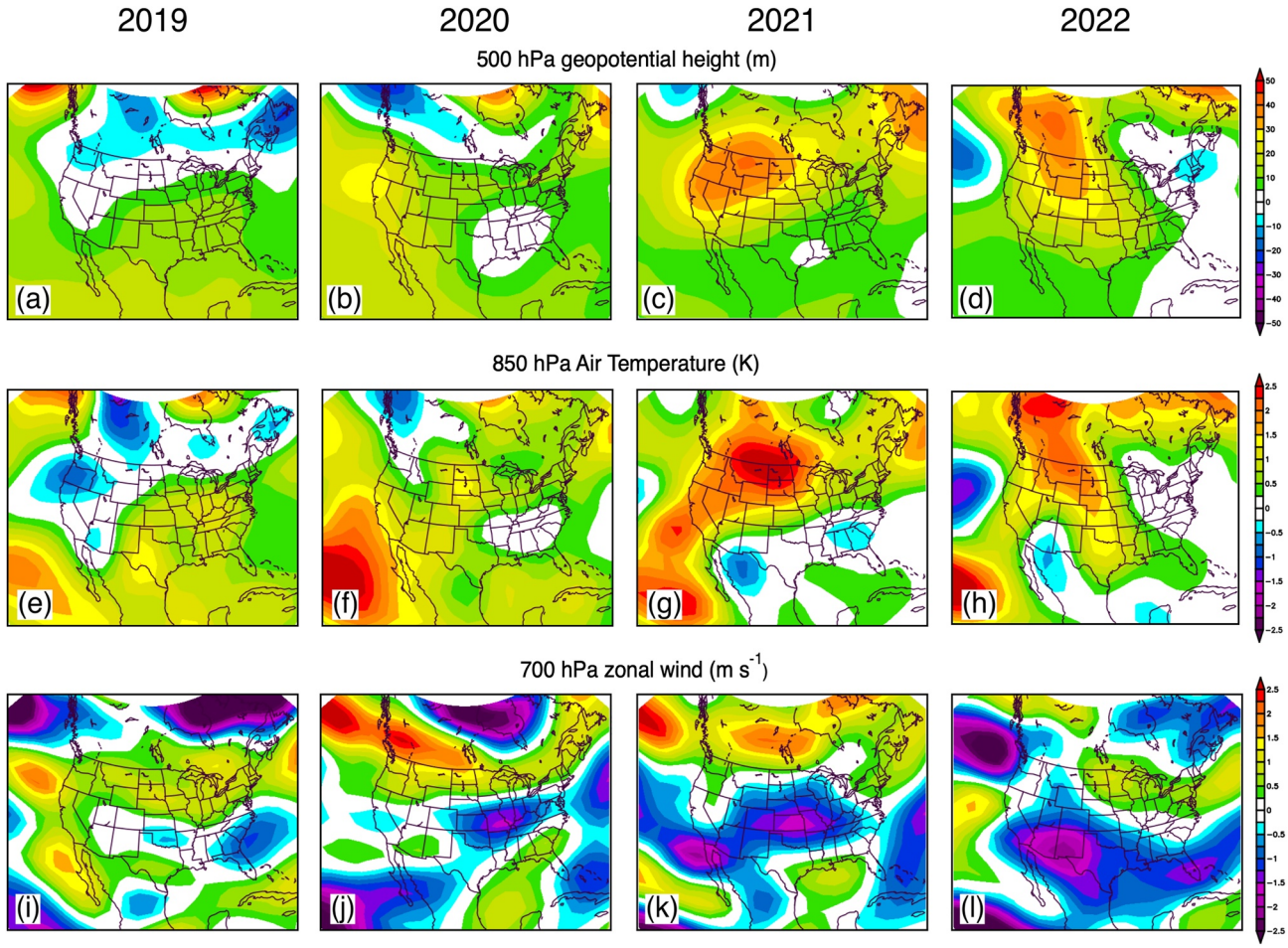

Figure 3. Mean summer (1 June–30 September) (top) 500 hPa geopotential height, (middle) 850 hPa temperatures, and (bottom) 700 hPa zonal wind anomalies (1991–2020 climatology) from the National Centers for Environmental Prediction/National Center for Atmospheric Research (NCEP/NCAR) Re-analysis. Images provided by the NOAA Physical Sciences Laboratory, Boulder Colorado from their website at https://psl.noaa.gov/.

(1991–2020) average. These conditions would have favored production of O_3 both in the nascent smoke plumes and further downwind as the PVOCs mingled with NO_x from anthropogenic sources. Previous studies (e.g., Reddy & Pfister, 2016) have shown that surface O_3 in the IMW, including Colorado, is positively correlated with 500 hPa heights, in part because high pressure aloft creates subsidence that suppresses cloud formation and weakens the zonal winds (Figure 3, bottom row) allowing O_3 and other pollutants to accumulate near the surface. Figure 3g shows that the summer of 2021 was especially hot in the PNW and IMW with both Seattle and Portland recording all-time highs of 42.2°C (108°F) and 46.7°C (116°F), respectively, on June 28 (NOAA NCEI, 2022). The highest temperature ever recorded north of 45°N (49.6°C or 121.3°F) was measured the following day (June 29) in Lytton, British Columbia, the day before the village was mostly destroyed by the eponymous Lytton Fire (ECCC, 2021). This unprecedented early heat wave (Bartusek et al., 2022; Thompson et al., 2022) exacerbated persistent drought conditions across the region, contributing to the major wildfires that burned across northern California and the PNW in late June and July (see Table S1 in Supporting Information S1). Figure 3 also shows that the mean temperatures were cooler than normal above the PNW and Northern California in 2019, a low wildfire year in the West, but warmer than normal along the West Coast in 2020 which was a record setting wildfire year in California (Table S1 in Supporting Information S1).

Table 1 shows that the average daily maximum surface temperatures and pressures recorded by the KDEN National Weather Service (NWS) station at Denver International Airport (DIA) (National Weather Service, 2023) were also higher in 2021 and 2022 than in the previous two years, and temperature records were broken in Denver on 13 consecutive days in mid and late June 2021 with daily highs in excess of 37.8°C (100°F) on three consecutive days

Table 1
Summary of June–September 2019–2022 Meteorological Observations From the National Weather Service (KDEN) Monthly Climate Reports

Parameter	2019	2020	2021	2022
T_{max} (°C)[a]	30.4 (2.8)	30.0 (2.0)	31.2 (2.0)	31.4 (2.3)
P (hPa)[a]	835.2 (1.1)	835.5 (1.9)	835.8 (1.0)	836.3 (1.4)
Rain (cm)	14.4	7.5	4.4	10.8
Sky cover				
Clear	26	27	44	30
partly cloudy	92	90	77	83
Cloudy	4	5	1	9
Smoke days	14	28	42	27
Thunder days	71	56	47	75
Lightning days[b]	80	60	56	73

[a]Mean of the daily maximum values. The standard deviations are shown in parentheses. [b]NLDN flash count above northern Front Range urban corridor (39.0°–40.8°N, 105.5°–104.5°W).

(15–17 June). The summer of 2021 was much drier (4.4 vs. 10.8 cm of rain), however, and had many more clear days (44 vs. 30) which would have favored photochemical production. The clear skies would also have decreased venting of O_3 and other pollutants by fair weather cumulus (Chen et al., 2012). There were also fewer thunderstorms which are particularly efficient at ventilating the boundary layer (Cotton et al., 1995) and fumigating it with cleaner free tropospheric air (Langford et al., 2010). Thunderstorms form above the high peaks of the Rocky Mountains by midday in most years and often pass over the Denver-Boulder area in the late afternoon and early evening as they track eastward (Schaaf et al., 1988). Surface O_3 usually drops precipitously when this happens and moderates the MDA8 concentrations at monitors that would otherwise have exceeded the NAAQS (Flocke et al., 2020). Table 1 shows that the KDEN observers reported audible thunder on only 47 days in 2021 and the National Lightning Detection Network (NLDN) recorded cloud-to-ground (CG) lightning strikes on only 56. Thunder was reported on only 8 of the 42 days when smoke was observed, which is consistent with studies (e.g. (Jiang et al., 2018),) showing that deep convection is suppressed by dispersed wildfire smoke.

Finally, weak zonal flow aloft allows the development of easterly upslope winds that can transport O_3 and other pollutants westward into the foothills (Fehsenfeld et al., 1983). These winds are part of the larger mountain-plains circulation that plays a major role in the evolution of high O_3 episodes in the Denver metropolitan area (Sullivan et al., 2016). The diurnal pattern is evident in Figure 4 which plots the July average wind probabilities from DIA (KDEN), Chatfield (CHAT), and the Rocky Flats-North (RFN) monitoring station near Boulder. The morning to early afternoon (08–15 MST) winds are shown on the left, and the late afternoon to evening (15–20 MST) winds on the right. The winds at DIA were weak and variable in the mornings, but usually had a northerly component. They strengthened and rotated clockwise to the east and south in the afternoon as the upslope flow developed. The winds at Chatfield were generally aligned along the adjacent South Platte River in the mornings and early afternoons, making this area a receptor for NO_x and VOCs from downtown Denver and other downstream sources. The larger red circles at RFN in Figures 4e and 4f show that there were more days with little or no wind (<1 m s^{-1}) in 2021 compared to the other years. These stagnant conditions allowed more of the locally produced O_3 to accumulate near the foothills.

4. Surface O_3 and $PM_{2.5}$ Measurements

4.1. Regional and Day-To-Day Variations

Time series of the 2021 MDA8 O_3 measurements from Chatfield (CHAT), La Casa (CASA), Rocky Flats-North (RFN), Rocky Mountain National Park (RMNP), and Greeley-Weld Tower (GRET) (US EPA, 2023a) surface monitors operated by the CDPHE and NPS are plotted in Figure 5a. These monitors (Table S2 in Supporting Information S1) span most of the DM/NFR and with the exception of RMNP have nearby or co-located $PM_{2.5}$ measurements (blue or violet filled circles in Figure 1b). The 2019 measurements from the Rocky Flats-North monitor (black staircase) are included for comparison. Each of these monitors exceeded the 2015 NAAQS on all but a few of the days between mid-July and mid-August of 2021, and all 16 of the regulatory O_3 monitors in the DM/NFR including the high elevation RMNP (2743 m a.s.l.) and Black Hawk (2633 m a.s.l.) stations simultaneously equaled or exceeded the NAAQS on 7 days: 12 July, 18–20 July, and 26–28 July. The 4 days with the highest MDA8 O_3 concentrations in the DM/NFR (15 June, 12 July, 22 July, and 8 September) are tagged in Figure 5a; these days are examined in more detail below. The highest concentrations were usually measured in the southern half of the DM/NFR at the Chatfield State Park (CHAT) monitor, which recorded an MDA8 of 96 ppbv on both 22 July and 8 September. The CHAT monitor also measured a 1-hr value of 109 ppbv and an MDA8 value of 101 ppbv on 12 July, but these measurements were not submitted to the AQS because of missing values on that day. The highest MDA8 on 15 June (94 ppbv) was measured by the Rocky Flats-North (hereafter Rocky Flats or RFN) O_3 monitor which is located about 25 km northwest of downtown Denver and 12 km southeast of Boulder. Table 2 shows that both of these monitors measured mean (median) MDA8 concentrations ($\pm 1\sigma$) of ≈66 (65)

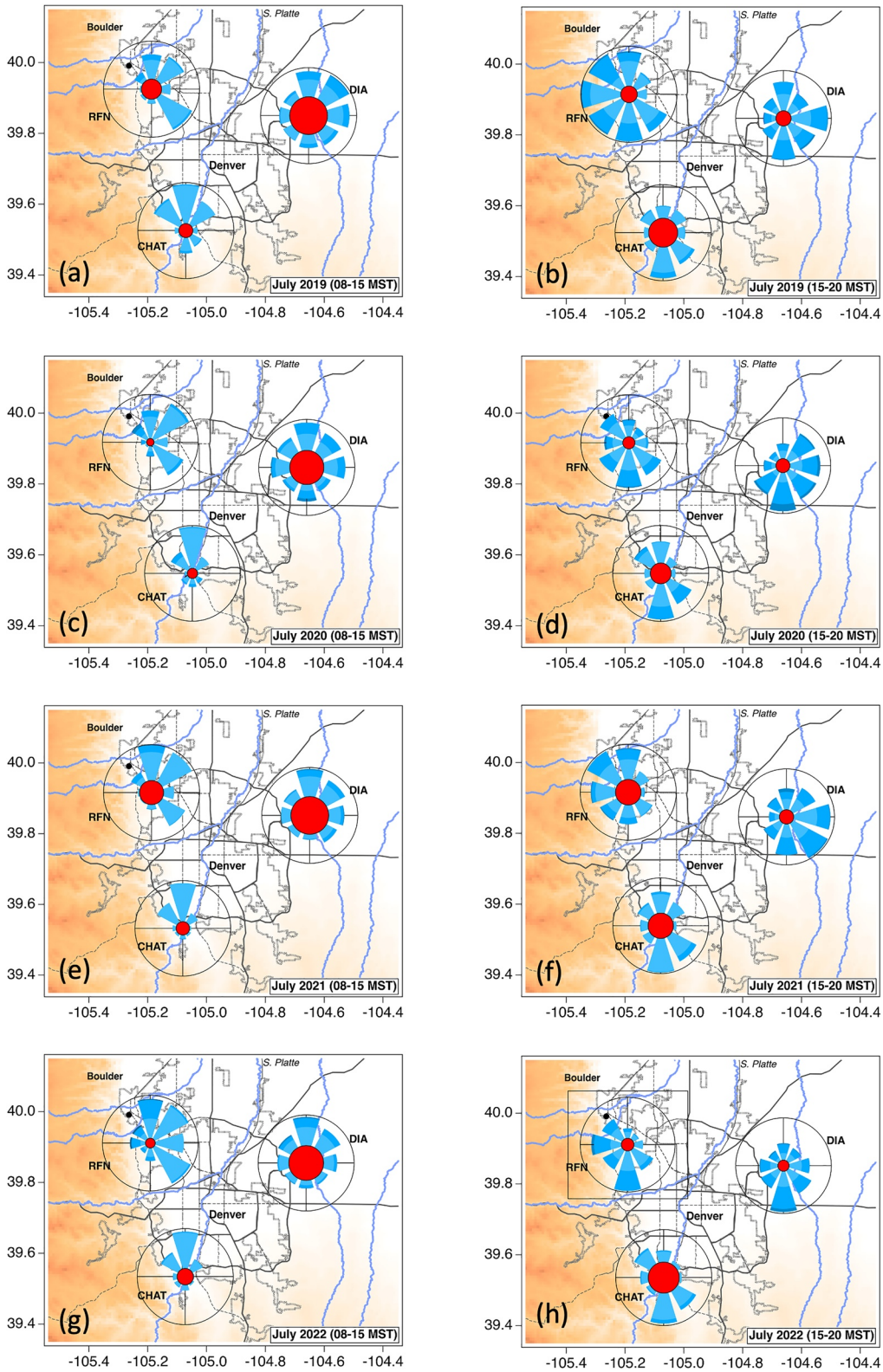

Figure 4. July average wind probabilities from DIA (KDEN), Chatfield (CHAT), and the Rocky Flats-North (RFN) monitoring station near Boulder. The morning to early afternoon (08–15 MST) winds are shown on the left, and the late afternoon to evening (15–20 MST) winds on the right. The red circles show the relative incidence of calm conditions (<1 m s^{-1}) and the blue colors correspond to wind speeds of 1–5, 5–10, 10–15, etc. m s^{-1}.

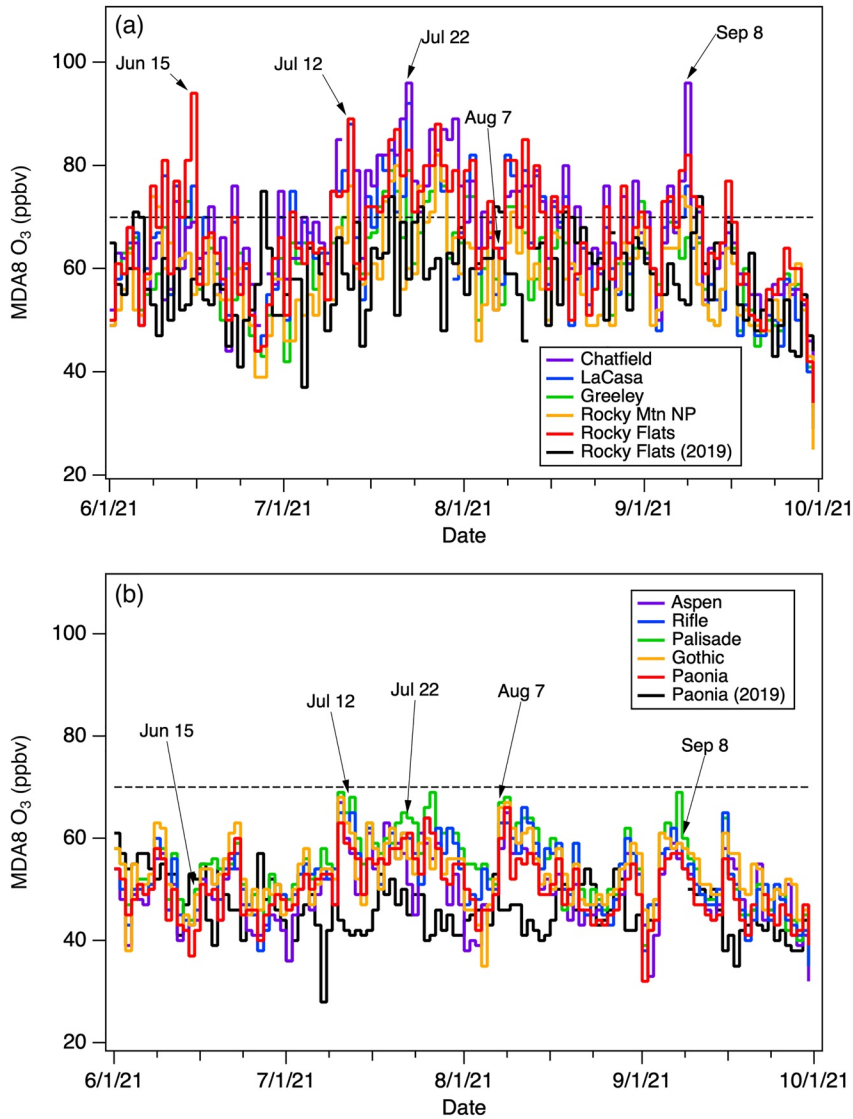

Figure 5. Time series of the MDA8 O_3 concentrations measured by five representative monitors in: (a) the DM/NFR (Greeley, Rocky Flats, La Casa, Rocky Mountain National Park, and Chatfield), and (b) the Western Slope (Aspen, Paonia, Palisade/Grand Junction, Gothic, and Rifle). The heavy black traces show the 2019 measurements from Rocky Flats or Paonia. The dashed black lines show the 2015 NAAQS. The 4 days with the highest measured MDA8 O_3 in the DM/NFR are tagged, as is 7 August, the day with the highest $PM_{2.5}$.

±11 ppbv in 2021, or about 8 ppbv higher than the ≈58 (58) ±8 ppbv measured in 2019 with more than twice as many exceedance days as any of the other 3 years. The average MDA8 measurements from 2020 to 2022 are only slightly larger than those from 2019, despite the much larger 4MDA8 O_3 concentrations in 2020.

Figure 5b plots the MDA8 O_3 measurements from four of the monitors on the Western Slope (WSLP). Paonia and Rangely were the only two WSLP monitoring sites with collocated O_3 and $PM_{2.5}$ measurements in 2019–2021 that were submitted to the AQS. The Rangely monitoring site lies in the oil and gas producing Weber Basin and nearly always measured higher O_3 and $PM_{2.5}$ than any of the other WSLP monitors; these measurements are not included in our analysis. The Paonia O_3 measurements were highly correlated ($R = 0.83$) with those from the high elevation CASTNET site at Gothic and thus can be used as a proxy for the regional baseline. The 2019 measurements from Paonia are also plotted in Figure 5b. Ozone pollution is generally much less severe on the sparsely populated WSLP which had a total 2020 population of about 586,000 compared to the more than 4.85 million on the Front Range (State of Colorado, 2023). The MDA8 O_3 concentrations measured at Aspen (ASPN),

Table 2
Mean, Median, and 1σ Values for the Paonia[a] (PAOA), Rocky Flats-North (RFN)/Boulder (BOU), and Chatfield (CHAT) MDA8 O_3 and 24-hr $PM_{2.5}$ Measurements (June–September)

Site	MDA8 O_3					$PM_{2.5}$		
	Mean	Median	Std. dev.	Days >70	4MDA8	Mean	Median	Std. dev.
PAOA								
2019	46.2	46	5.5	0	57	4.7	4.6	1.2
2020	47.5	47.5	6.8	0	61	7.6	5.4	5.9
2021	50.2	50	6.1	0	61	9.9	7.3	8.2
2022[a]	45.0	45	7.2	0	59	5.0	4.1	3.4
RFN/BOU								
2019	58.2	58.5	7.9	8	72	6.2	5.6	3.1
2020	60.1	59	10.3	16	84	8	5.9	6.4
2021	66.1	65	11.1	47	87	10.9	9.2	7.1
2022	60.1	62	10.6	21	78	6.0	5.5	2.7
CHAT								
2019	58.5	58	8.4	10	78	6.2	6.2	1.6
2020	58.3	58	11.3	13	83	10.4	6.7	9.4
2021	66.4	65	11.3	41	89	14	11.1	10.2
2022	59.0	60	11.3	17	78	5.6	5.0	2.6

[a]2022 measurements are from Aspen. All of the 2022 measurements are preliminary.

Paonia (PAOA), Palisade (PAL), and Rifle (RIFL) were accordingly much lower and similar to those measured by the remote high elevation (2900 m a.s.l.) CASTNET (https://www.epa.gov/castnet) monitor at Gothic that is included for reference. The O_3 concentrations on the WSLP were always much lower than those measured in the DM/NFR, but were still higher in 2021 than in 2019 with mean (median) MDA8 concentrations of 50 (50) ±6 ppbv at Paonia (pop. 2,700) compared to 46 (46) ±5 ppbv (Table 2). The mean (median) MDA8 concentrations at Paonia in 2020 were also elevated compared to 2019, possibly because of the nearby Pine Gulch fire. The highest MDA8 O_3 measured in the WSLP in 2021 was 76 ppbv which was recorded by the Rangely monitor on 9 August.

Figures 6a and 6b are similar to Figures 5a and 5b, but plot the 24-hr averaged measurements from the collocated or proximate $PM_{2.5}$ monitors (blue or violet filled circles in Figure 1b). The downtown Boulder (BOU) monitor is located ≈13 km NW of Rocky Flats. The 2019 measurements from the Boulder and Paonia monitors are included in Figures 6a and 6b, respectively, for comparison. The DM/NFR and WSLP $PM_{2.5}$ measurements appear very similar with all of the time series increasing abruptly on 10 July when smoke from the Bootleg Fire in Oregon, the first of the major West Coast wildfires started by lightning on 6 July, reached Colorado, and peaking on 7 and 8 August, a few days after a dry cold front initiated a period of explosive growth in the Dixie Fire in northern California. The most significant differences between the time series is on 1 and 2 August when smoke from wildfires in Manitoba and Ontario reached the Front Range, but was too low to cross the Rockies into the Western Slope. Both plots show smaller peaks on 12 July, 24 and 25 July, 30 and 31 August, and 8 September with substantial concentration differences on 12 July and 8 September. The DM/NFR peaks sometimes lagged the WSLP maxima as the smoke moved east, but the haze was fairly uniformly dispersed across the northern half of the state on most days between 10 July and 30 September. This is reflected in the strong correlation (La Casa = 3.9 ± 0.9 + [0.98 ± 0.06]*Paonia, $R^2 = 0.76$) between the 24-hr $PM_{2.5}$ measurements from La Casa and Paonia (excluding 1 and 2 August).

Figure 6a also plots (right axis) the total organic carbon (TOC) and bulk potassium (K) concentrations from filter samples collected at CASA every third day for the NCORE multipollutant network (Scheffe et al., 2009). Potassium is often used as a marker for biomass burning (Pachon et al., 2013) and the high degree of correlation between the speciated TOC ($R^2 = 0.99$) and K^+ ($R^2 = 0.84$) measurements and the total $PM_{2.5}$ concentrations suggests that most of the particles collected at La Casa were from wildfire smoke, including those sampled in

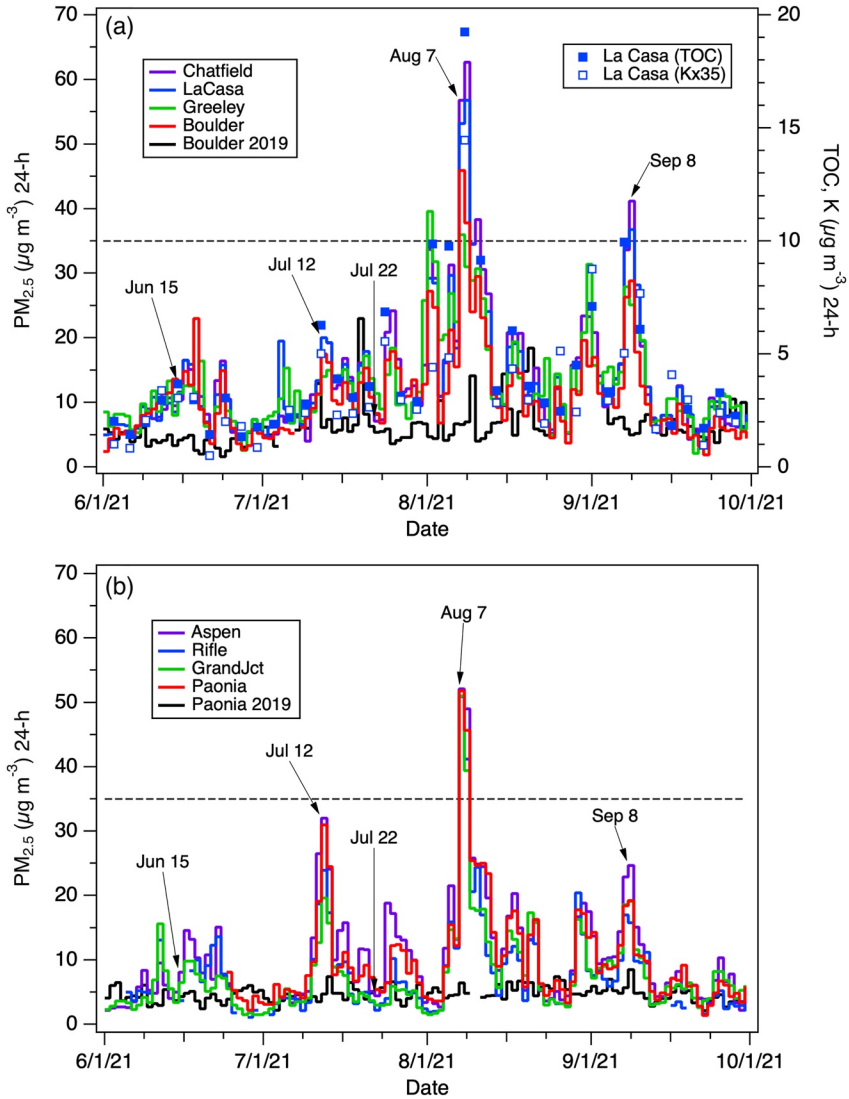

Figure 6. 24-hr $PM_{2.5}$ concentrations from the (a) DM/NFR, and (b) WSLP, regulatory monitors shown in red or purple in Figure 1b. The heavy black traces show the 2019 measurements from Boulder (top) and Paonia (bottom). The dashed black lines represent the 24-hr NAAQS of 35 μg m^{-3}. The isolated peaks in the 2019 Boulder measurements (e.g., 19 July and 20 August) were caused by short-lived (1–2 hr) spikes attributed to a nearby source. Panel (a) also shows the K and TOC measurements made every third day at La Casa (right axis); note that the K concentrations have been scaled by a factor of 35. The days with the highest MDA8 O_3 values (cf. Figure 5) in each airshed are tagged.

mid-June while the Telegraph Fire was still active, but before the start of the large West Coast fires. Smoke distributions above Colorado on the four peak O_3 days can also be seen in the visibility camera and satellite images (Figure S1 in Supporting Information S1), HRRR-smoke analyses (Ahmadov et al., 2017), and HYSPLIT back trajectories (Stein et al., 2015) (Figures S3 and S4 in Supporting Information S1). Histograms of the Paonia, Rocky Flats/Boulder, and Chatfield measurements (Figure 7) show that high $PM_{2.5}$ and O_3 concentrations were measured much more frequently in 2021 than in 2019, 2020, and 2022.

The MDA8 O_3 concentrations from the Paonia, Rocky Flats, and Chatfield monitors are plotted against the corresponding 24-hr $PM_{2.5}$ concentrations in Figure 8. The Boulder/Rocky Flats (Figure 8a) and Chatfield (Figure 8b) measurements are plotted separately for clarity. The July measurements are highlighted in each plot for emphasis. The dotted line shows the MDA8 O_3 to 24-hr $PM_{2.5}$ relationship derived by Buysse et al. (2019) from an analysis of the July to September measurements from 18 western U.S. cities between 2013 and 2017; the yellow diamonds show the binned Denver measurements from that study. The curve is based on measurements from both smoky

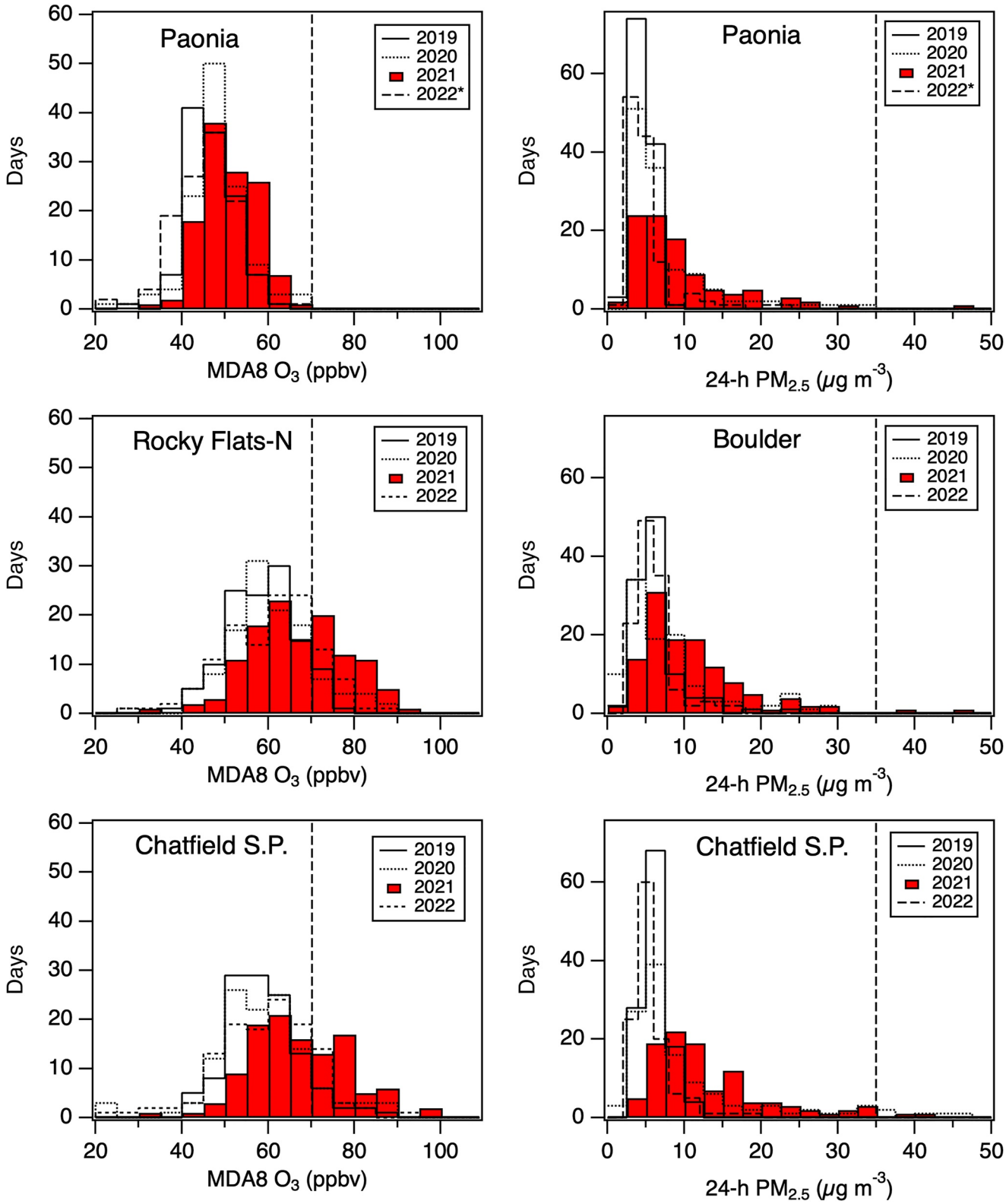

Figure 7. Histograms of the 1 June–30 September (2019–2022) MDA8 O_3 and 24-hr $PM_{2.5}$ measurements from: (a and b), Paonia, (c and d), Rocky Flats and Boulder, and (e and f), Chatfield. The O_3 and $PM_{2.5}$ measurements from Aspen are substituted for the unavailable Paonia 2022 measurements; all of the 2022 measurements should be considered preliminary.

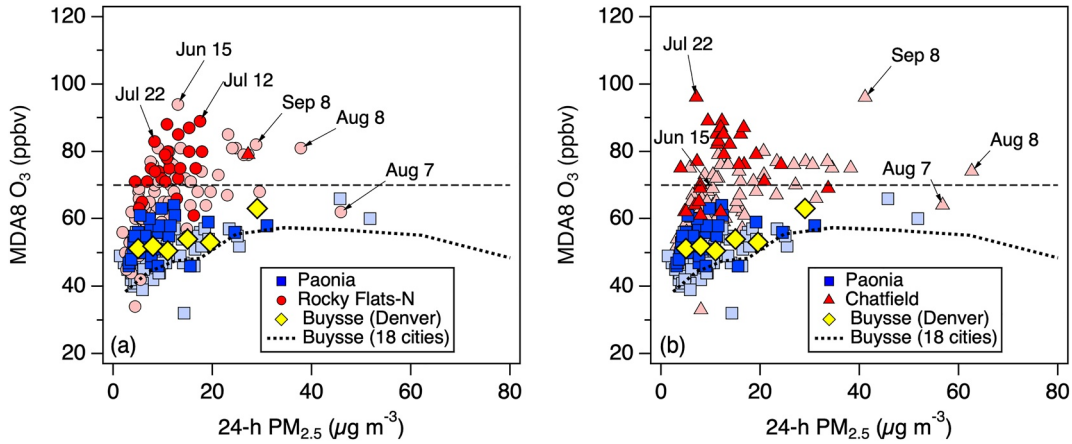

Figure 8. (a) Scatter plot comparing MDA8 O_3 and 24-hr $PM_{2.5}$ measurements from Rocky Flats/Boulder (filled red circles) and Paonia (filled blue squares). The darker colors highlight the July measurements. The dashed line represents the 2015 NAAQS and the 5.7 dotted line shows the mean relationship derived by Buysse et al. (2019) using the 2013–2017 measurements from 18 wildfire-impacted cities in the Western U.S. The yellow diamonds are the binned Denver measurements from that study. (b) Same as (a), but with the Chatfield data including the preliminary 6–13 July measurements. The $PM_{2.5}$ measurements from 11 to 12 July are missing.

and smoke-free periods and most of the Paonia measurements lie near the curve, which turns over at high smoke loadings, presumably because of gaseous deposition to the smoke particles or attenuation of the actinic flux. The 2021 Chatfield and Rock Flats measurements generally lie well above this curve because most of the local O_3 production is unrelated to the wildfire smoke, but were much closer during the heavy smoke episode of 7 and 8 August when the local production was diminished.

4.2. Smoke in Northern Colorado

Satellite images show that the dispersed smoke that drifted into Colorado from the northwest often blanketed the entire northern half of the state in July and August (see Supporting Information S1). This is reflected in the strong correlations between the 24-hr $PM_{2.5}$ Paonia measurements in Figure 5b and those from La Casa ($R^2 = 0.76$) and Boulder ($R^2 = 0.78$) in Figure 5a. More than 45% of the June-September daily averages (70% in July) exceeded 8 μg m^{-3} which we use as a threshold for the presence of smoke. This threshold is based on the mean $PM_{2.5}$ loadings of 5.9 ± 1.2 and 6.2 ± 0.8 μg m^{-3} measured at Boulder in the low wildfire years of 2019 and 2022 (cf. Figure 9c) and the intercept (6.2 ± 1.06 μg m^{-3}) of a linear regression fit between the La Casa $PM_{2.5}$ and K^+ measurements plotted in Figure 6a. Note that this objective criterion identifies significantly more days with smoke influences than the subjective visual assessments used by the KDEN observers (cf. Table 1). The drifting haze changed relatively little from hour-to-hour and thus appears as a constant offset in the diurnally averaged hourly $PM_{2.5}$ measurements from the Paonia, Boulder, and Chatfield monitors plotted in Figure 9. This figure displays the summer (1 June to 30 September) averages on the left and the July only averages on the right. The Paonia measurements were discontinued in May of 2022. The diurnal averages are listed in the inset boxes. We plot the mean rather than median values since these are more directly relatable to the MDA8 measurement and the error bars show typical standard deviations for the early morning and midday averages. The plotted error bars are offset and the remaining error bars omitted for clarity. The year-to-year differences between the averaged measurements are much smaller than the standard deviations and are probably a better indicator of the uncertainties. The solid lines in the plots on the left show that the summer mean particulate loadings were similar at each of the monitoring sites in the low wildfire years (e.g., 5.9 ± 1.2 μg m^{-3} in 2019 and 6.2 ± 0.8 μg m^{-3} in 2022 in Boulder) with larger mean concentrations in the high wildfire years (e.g., 9.5 ± 0.9 μg m^{-3} in 2020 and 11.0 ± 0.8 μg m^{-3} in 2021 in Boulder). The mean $PM_{2.5}$ at all three sites was highest in 2021 even though 2020 was a record-setting wildfire year for both California and Colorado. This is because most of the large 2020 wildfires did not start until August and September and thus did not affect the June and July measurements.

The dotted black lines in all of Figure 9 plots show the mean reference concentrations estimated from measurements made during periods without wildfires. For Boulder and Chatfield, this is the average of the 2019 and

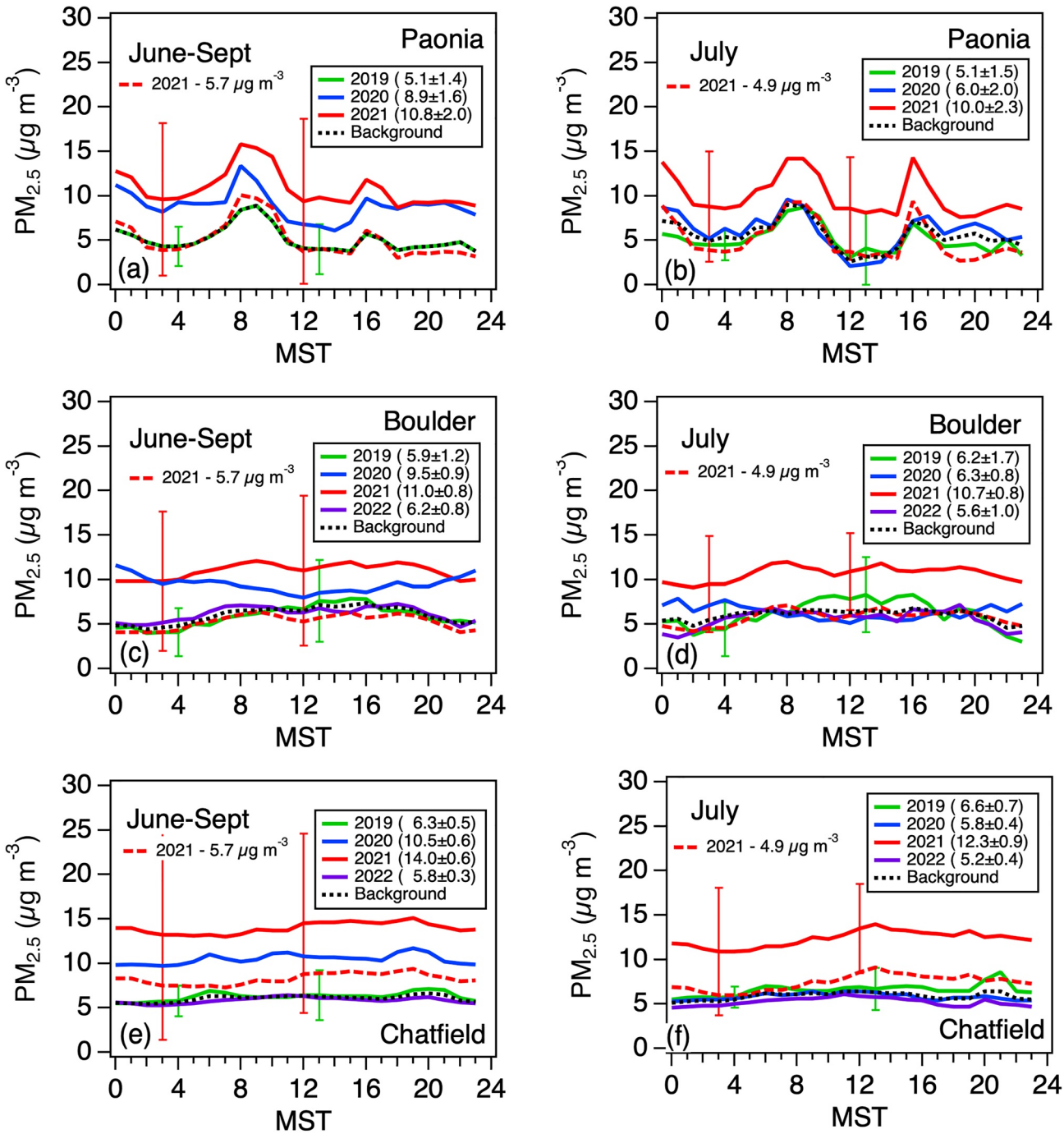

Figure 9. Hourly $PM_{2.5}$ averaged over the summer (1 June–30 September, left) and the month of July (right) from Paonia (top), Boulder (middle), and Chatfield (bottom) for the years 2019–2022. The 2022 Paonia measurements were unavailable. The dotted black lines show the smoke-free background described in the text. The dashed red lines show the 2021 measurements offset by the diurnally averaged Paonia enhancements of 5.7 μg m^{-3} (left) and 4.9 μg m^{-3} (right) from Table 3. The error bars show typical standard deviations of the 2019 and 2021 measurements. The remaining error bars are omitted for clarity.

2022 measurements with the 2020 measurements included for the June and July averages. For Paonia, the 2019 measurements are used for the summer, August, and September, with the 2020 measurements added in June and July. The differences between the mean $PM_{2.5}$ concentrations measured at Paonia, Boulder, and Chatfield in 2021 and the corresponding reference values are summarized in Table 3. The suitability of using the data from 2019 to 2022 as reference measurements was confirmed by a day-by-day examination of satellite imagery and $PM_{2.5}$ maps, which showed no days when there was a significant wildfire influence (*i.e.*, visible smoke and more than

Table 3
Diurnally Averaged $PM_{2.5}$ and O_3 Enhancements Above "No Smoke" Periods

	June[a]	July[a]	August	September	Summer
$PM_{2.5}$ (μg m^{-3})					
Paonia	−0.4 (2.1)	4.9 (1.6)	9.7 (1.7)	3.2 (1.8)	5.7 (0.7)
Boulder	1.9 (1.9)	4.6 (0.6)	9.2 (1.0)	2.8 (1.0)	5.0 (0.4)
Chatfield	3.9 (0.6)	6.4 (0.8)	14.7 (1.3)	5.2 (0.8)	7.9 (0.6)
O_3 (ppbv)					
Paonia	−0.9 (0.7)	8.2 (2.5)	2.6 (1.3)	2.3 (1.3)	2.8 (0.6)
Rocky Flats	3.0 (2.3)	10.5 (2.2)	5.3 (1.0)	6.6 (0.6)	6.1 (1.0)
Chatfield	2.2 (2.8)	12.8 (4.0)	4.2 (1.1)	5.2 (1.4)	5.3 (1.5)

[a]Reference values includes 2020 measurements. The standard deviations are shown in parentheses.

8 μg m^{-3} of $PM_{2.5}$ (24-hr) at 3 or more monitors in either the DM/NFR or WSLP) during the summer (1 June–30 September) of 2019, and only 1 day in 2022. The latter was on 13 June when smoke from the Pipeline and Haywire Fires burning to the north of Flagstaff, AZ passed diagonally across Colorado and elevated surface $PM_{2.5}$ in both air basins.

Table 3 suggests that the dispersed smoke haze increased the 2021 $PM_{2.5}$ concentrations in Paonia by an average of 5.7 ± 0.7 μg m^{-3} above the no smoke reference values over the summer and by 4.9 ± 1.6 μg m^{-3} in July. The dashed red lines in all of the plots show the respective 2021 measurements with the Paonia enhancement subtracted. Figures 9c and 9d show that the Boulder measurements converge with those from the other years when the mean 2021 Paonia concentration is subtracted. This supports the above conclusion that the WSLP and DM/NFR were similarly impacted by the dispersed smoke haze in 2021. The summer and July $PM_{2.5}$ enhancements measured by most of the other Front Range monitors were similar to those in Boulder (e.g., La Casa (6.0 and 4.6 μg m^{-3}) and Greeley (5.5 and 4.6 μg m^{-3}). The only measurements that did not converge with the reference values were those from the Chatfield monitor which are plotted in Figure 9e. Much of this difference was caused by the heavy smoke event of 7 and 8 August (cf. Figure 6a), but there is still a small difference when only the July measurements are plotted (Figure 9f).

4.3. Smoke Impact on O_3

Figure 10 is similar to Figure 9, but plots the corresponding O_3 measurements with the smoke free reference concentrations calculated as before. The enhancements relative to the reference values are also summarized in Table 3. The inset boxes show the 10 to 18 MST 8-hr averages (±1σ) which differ slightly from the values in Table 2 because of shifts in the timing of the daily O_3 maxima and the rounding and truncation rules used in the MDA8 calculations. The average enhancements at Paonia were −0.9 ± 0.7, 8.2 ± 2.5, 2.6 ± 1.3, and 2.3 ± 1.3 ppbv, in June, July, August, and September, respectively, with a mean enhancement of 2.8 ± 0.6 ppbv over the entire summer. Since there is relatively little photochemical production of O_3 in the Paonia area, these values represent our best estimates of the pyrogenic O_3 contribution to the surface concentrations in northern Colorado during the summer of 2021. Table 3 shows that the summer average 24-hr O_3 enhancements were several ppbv higher at Rocky Flats and Chatfield than at Paonia, and the offset curves for July in Figures 10d and 10f show that the peak afternoon concentrations were ≈5 ppbv higher, on average, than the reference values at Rocky Flats and ≈12 ppbv higher at Chatfield. The mean MDA8 concentrations were ≈4 ppbv higher (63.9–60.2 ppbv) at Rocky Flats in July and ≈9 ppbv higher (68.8–59.6 ppbv) at Chatfield. These enhancements show the local O_3 contribution and include any O_3 formed in the reactions of PVOCs with NO_x from local sources.

Figure 11 shows the July 2021 (solid red lines) and reference values (dotted black) O_3 measurements from Rocky Flats (top row) and Chatfield (middle row) plotted in Figure 10, but with the 2021 measurements also separated into those made on days when smoke was present ($PM_{2.5}$ >8 μg m^{-3}, dashed red line) and not present (<6 μg m^{-3}, dotted red line). The pyrogenic O_3 contribution (cf. Section 4.3) has been subtracted in the panels on the right. The "smoke" measurements from both monitors lie slightly above the monthly averages as would be expected. The "no smoke" measurements lie closer to the reference values, but are rather noisy because of their small sample sizes. Figure 11b shows that the Rocky Flats measurements from the "smoke" and "no smoke" days become similar when the pyrogenic O_3 contribution is subtracted suggesting that there was no significant production of O_3 from PVOCs in the Boulder area. All three curves lie slightly above the reference values, which would give an upper limit of 2–3 ppbv (62.8–60.2 ppbv) for the local MDA8 enhancement due to smoke, but this difference may not be statistically significant. The Chatfield measurements from the "smoke" days in Figure 11d remain well above the reference values, however, and the difference between the dashed red and dotted black curves corresponds to an increase in the Chatfield MDA8 of ≈12 ppbv (72.0–59.6 ppbv), on average, on smoky days in July. As discussed in Section 3, these higher O_3 concentrations at Chatfield are consistent with the observed wind patterns. The northerly winds in the mornings and early afternoons would have transported NO_x from downtown Denver directly to Chatfield along the South Platte River where it would have been available to react with any

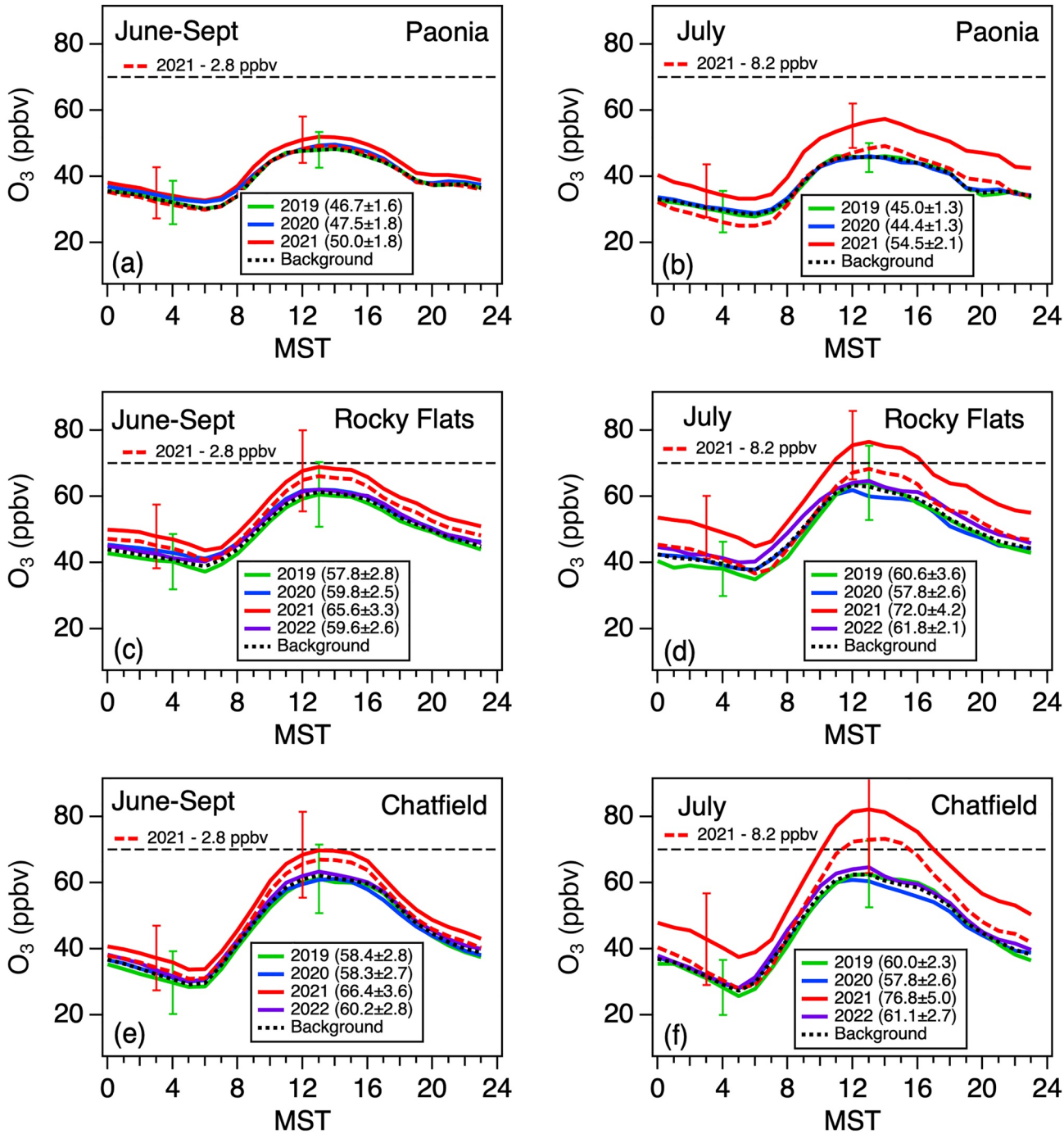

Figure 10. Same as Figure 9, but for O_3. The dashed red lines show the 2021 measurements offset by the diurnally averaged Paonia enhancements of 2.8 ppbv (left) and 8.2 ppbv (right) from Table 3. The preliminary Chatfield measurements from 6 to 13 July are used since they meet the EPA accuracy requirements of ±15%, but did not meet the CDPHE standards for final data. The curve is essentially unchanged if these data are omitted.

PVOCs in the smoke. Also, the more northerly afternoon winds in 2021 (Figure 4f) would also have kept much of the NO_x and O_3 formed in Denver away from Boulder and Rocky Flats.

The clear skies and lack of deep convection in 2021 may also have enhanced the MDA8 concentrations by allowing O_3 that might otherwise have been vented into the free troposphere or dispersed by thunderstorm downdrafts in the late afternoon to remain near the surface. Figures 11e and 11f are similar to Figures 11c and 11d, but show the July Chatfield measurements divided into days when CG lightning strikes were (10 days) and were not

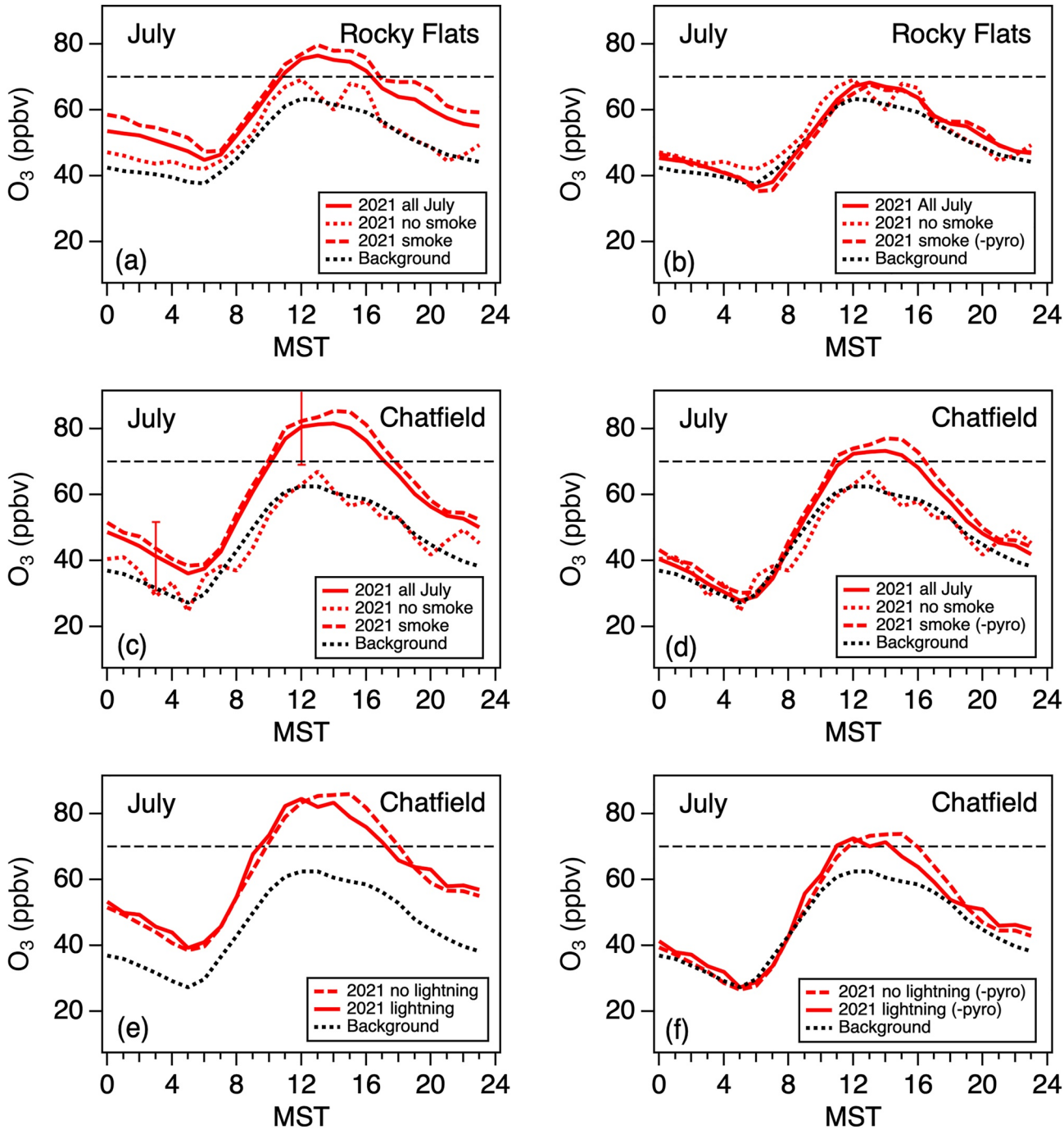

Figure 11. (a) Diurnal plot showing the July 2021 O_3 measurements from Rocky Flats (solid red line) and corresponding background curve (dotted black line) from Figure 10d. The dashed and dotted red lines parse the 2021 measurements into "smoke" and "non smoke" days. (b) Same as (a), but showing the offset Rocky Flats measurements. (c) Diurnal plot showing the July 2021 O_3 measurements from Chatfield (solid red line) and corresponding background curve (dotted black line) from Figure 10d. (d) Same as (c), but showing the offset Chatfield measurements. (e and f) Same as (d and e), but parsed into "lightning" and "no lightning" days.

(21 days) detected within 25 km of the monitor. The late afternoon concentrations (15–18 MST) were 3–7 ppbv lower on days with lightning, and the MDA8 concentrations ≈2 ppbv lower (67.0 ± 4.9 vs. 69.0 ± 5.2 ppbv). Since many of the smoky days were also lightning free, a similar analysis was performed using the 2022 measurements which gave a very similar result. The days with lightning were, of course, cloudier in the afternoons, but the similar midday peaks on the days with and without lightning in Figures 11e and 11f suggest that there wasn't a significant decrease in O_3 production on the days with lightning.

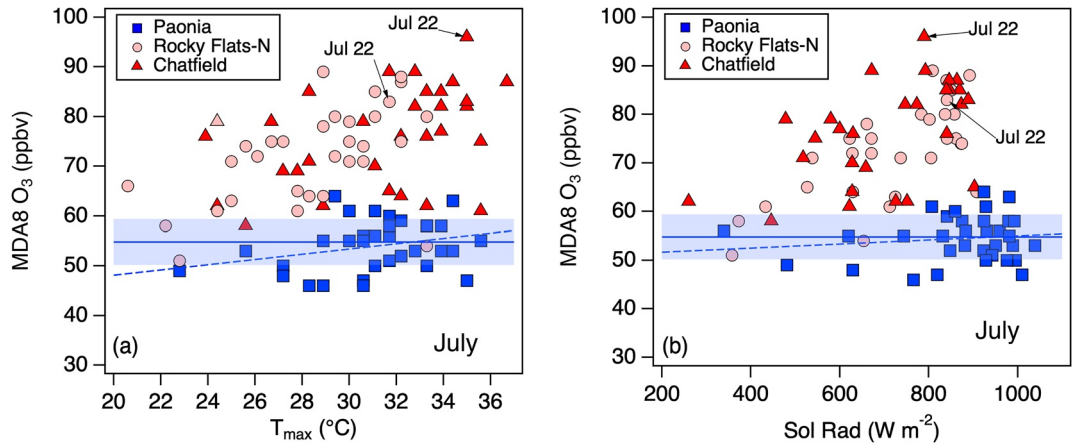

Figure 12. (a) Relationship between MDA8 O_3 and maximum daily surface temperature measured by a collocated sensor during July 2021. (b) Relationship between MDA8 O_3 and mean 12–16 MST solar flux. The Rocky Flats O_3 is plotted against measurements from a collocated sensor. The Paonia and Chatfield O_3 is plotted against measurements from the Carpenter Peak (CPTC2) and Jay (JAYC2), respectively, Interagency Remote Automatic Weather Stations (RAWS) operated by the BLM and USFS and downloaded from Mesowest (https://mesowest.utah.edu). The solid blue lines and shading show the means and standard deviation of the Paonia measurements and the dashed blue lines the linear regressions.

The regional differences in local O_3 production are also apparent in Figures 12a and 12b, which plot the MDA8 O_3 concentrations from the Paonia, Boulder/Rocky Flats, and Chatfield monitors as a function of daily maximum temperature and solar flux, respectively, the dominant drivers of the photochemistry (Sillman & Samson, 1995). These figures confirm that local O_3 production was negligible at Paonia on the sparsely populated WSLP. Figure 12a also shows that the higher O_3 at Chatfield may also have been due in part to warmer temperatures, as the daily maxima in July 2021 were about 3°C higher (31.4 vs. 28.5°C) on average than those measured at Rocky Flats.

5. Lidar O_3 and Backscatter Measurements

Wildfire smoke and pyrogenic O_3 can be transported hundreds or even thousands of km in the free troposphere before being entrained into the boundary layer far downwind (Johnson et al., 2021; Lin et al., 2021; McKeen et al., 2002). In-situ measurements of pyrogenic O_3 in the free troposphere have rarely been made outside of aircraft-based field campaigns, but O_3-rich smoke plumes have also been detected by ground-based lidars belonging to the NASA-sponsored Tropospheric Ozone Lidar Network (TOLNet) (Dreessen et al., 2016; Kuang et al., 2017; Langford et al., 2020, Johnson et al., 2021; Wang et al., 2021) and the relationship between the aerosol backscatter (β) and O_3 in the smoke can be used to estimate the amount of pyrogenic O_3 above the lidar (Langford et al., 2020). Here we use the measurements from the Tunable Optical Profiler for Aerosol and oZone (TOPAZ) lidar (Alvarez et al., 2011; Langford et al., 2019), located at the NOAA David Skaggs Research Center (DSRC) to characterize the smoke and O_3 distributions above Boulder. This lidar measures backscatter (β) and ozone profiles from 0.03 to ≈8 km a.g.l. every 10 min for up to 16 hr a day. The lidar was usually operated on ozone action days and other times when high O_3 was anticipated and a total of 1853 profiles were acquired on 37 of the 122 days from 1 June to 30 September (≈30% coverage) including all four of the peak O_3 days tagged in Figure 5a. Total uncertainties in the 10-min O_3 retrievals are estimated to increase from ±3 ppbv below 4 km to ±10 ppbv at 8 km. The backscatter measurements are most sensitive to particles similar in size to the laser wavelength (*i.e.*, 0.3 μm). Measurements from the NREL AERONET sun photometer (Figure S2 in Supporting Information S1) show this is close to the mean diameter of the aged wildfire smoke (Nikonovas et al., 2015). More details about the TOPAZ system and comparisons between the low elevation angle retrievals and nearby surface measurements (Figure S5 in Supporting Information S1) are provided in Supporting Information S1.

Figure 13a compares the TOPAZ column mean backscatter between 0.03 and 4 km a.g.l. with the 340 nm aerosol optical depth (AOD) measurements from the NREL sun photometer ≈30 km to the south (see Supporting Information S1). The measurements are in excellent agreement with a squared Pearson regression coefficient of $R^2 = 0.81$. Note that there were no lidar measurements during the 7 and 8 August smoke event. Figure 13b

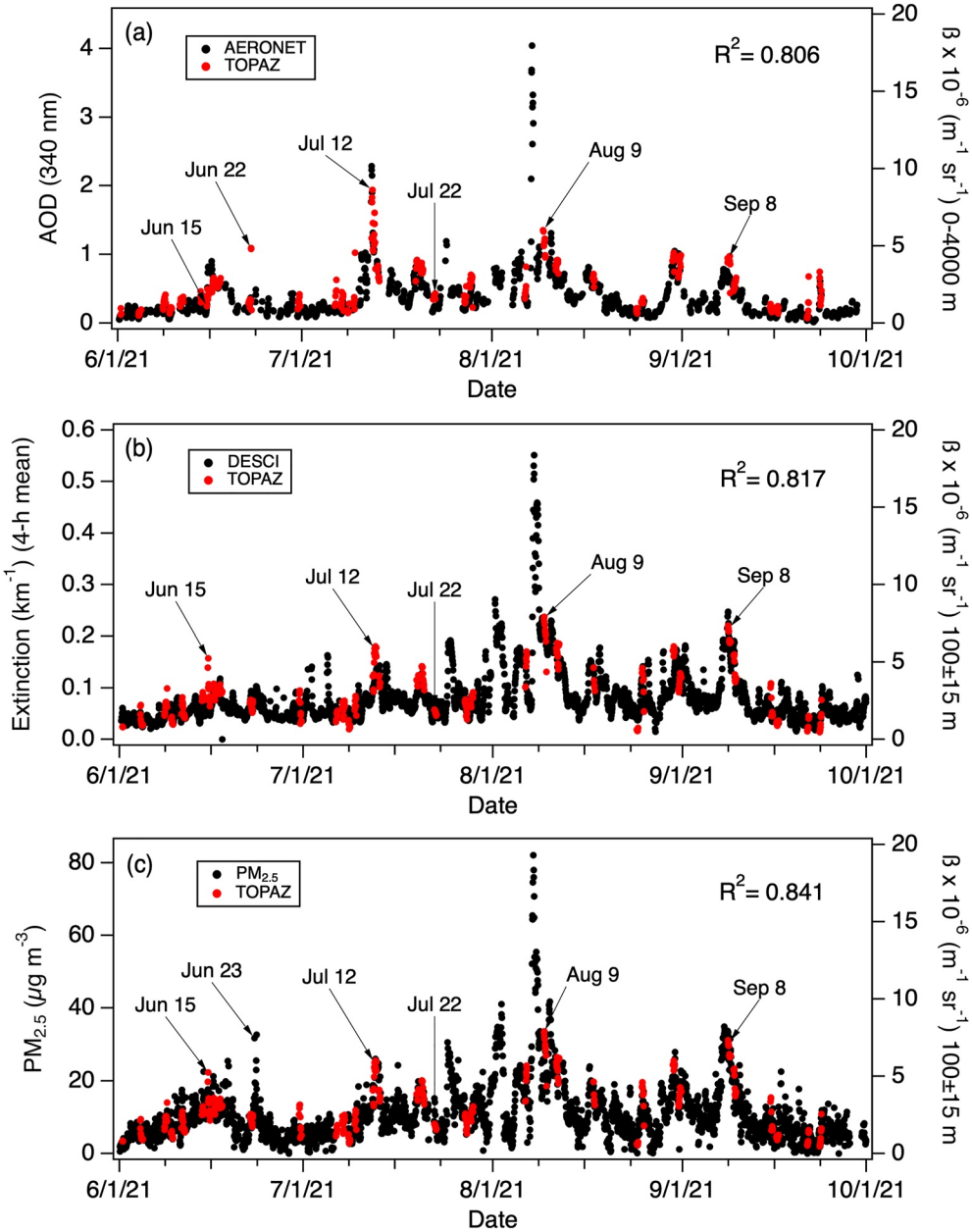

Figure 13. Time series plots comparing: (a) 340 nm AERONET aerosol optical depth (direct sun) measurements at NREL and mean column TOPAZ backscatter at 294 nm. (b) Horizontal extinction measurements from downtown Denver and mean TOPAZ backscatter at 100 ± 15 m a.g.l. (c) Boulder (BOU) $PM_{2.5}$ mass concentrations and mean TOPAZ (red) backscatter at 100 ± 15 m a.g.l (see Figure 9d). The TOPAZ and AERONET measurements have been interpolated to the 1-hr time base.

compares the TOPAZ backscatter at 100 ± 15 m a.g.l. with the extinction measurements along a 2.5 km path corresponding to the view of downtown Denver seen by the visibility camera (cf. Figure S1 in Supporting Information S1); these measurements are also seen to be in excellent agreement ($R^2 = 0.82$). The 10-min lidar profiles were interpolated to the 1-hr time base used by the surface measurements for these comparisons. The high degree of correlation between these three physically separated remote sensing measurements shows the homogeneity of the dispersed smoke haze above the Denver-Boulder area. The final panel (Figure 13c) compares the 100 m a.g.l. TOPAZ backscatter measurements with the hourly $PM_{2.5}$ measurements from the BOU monitor. These plots show that the bulk extinction-to-backscatter (lidar ratio) and backscatter-to-mass ratios were generally similar for the smoke from the different fires. The apparent outlier in the TOPAZ measurements from 22 June in Figure 13a was

caused by an elevated smoke plume from the nearby Muddy Slide Fire that reached Boulder in the late afternoon after the last direct sun AOD measurements in Golden.

Time-height curtain plots showing the particle backscatter (β) and O_3 above Boulder on the four peak O_3 days are displayed in Figure 14. These 4 days include 2 with smoke (12 July and 8 September), and 2 with little or no smoke (15 June and 22 July). Figure S4 in Supporting Information S1 shows roughly analogous cross-sections from the HRRR-Smoke model. The dashed black line in each curtain shows the hourly local mixed layer height (MLH) inferred from measurements of the vertical velocity variance and backscatter by an autonomous near-infrared (1.54 μm) Doppler lidar (Choukulkar et al., 2017) located on the roof of the DSRC. The DSRC is located adjacent to the Boulder foothills and the complex terrain, together with daytime sampling gaps due to instrument overheating, caused the automated MLH algorithm developed for the Doppler lidars (Bonin et al., 2018) to produce ambiguous results so the MLHs were determined subjectively from the backscatter measurements.

The curtain plots show very different smoke distributions on the four highest surface O_3 days (cf. Figure 5a) that are consistent with the surface measurements. The measurements from 15 June (Figures 14a and 14b) show light smoke and high O_3 concentrated very near the surface. The largest O_3 and β enhancements were measured on 12 July. These measurements (Figures 14c and 14d) show heavy smoke with a coincident O_3 maximum above the boundary layer in qualitative agreement with the HRRR-smoke transect in Figure S4b in Supporting Information S1. The peak β values ($\approx 1.6 \times 10^{-5}$ sr^{-1} m^{-1}) on 12 July were comparable to those measured in smoke from the 2016 Soberanes Fire in California which was a mixture of fresh smoke embedded in a diffuse haze that had circulated around the San Joaquin Valley for several days (Langford et al., 2020). Figure 14c also appears to directly show the entrainment of smoke (and O_3) from the lower free troposphere (LFT) by the growing boundary layer around 16:00 MST (see Data Availability Statement). The measurements from 22 July (Figures 14e and 14f) show high O_3, but no smoke at all between the surface and about 2 km a.g.l. Finally, Figures 14g and 14h show that there was moderate smoke and high O_3 on 8 September both in and above the boundary layer with a layered structure that is also qualitatively similar to the HRRR-smoke transect (Figure S4d in Supporting Information S1). This was the only time a well-defined smoke layer was observed in 37 days of lidar measurements.

5.1. Lidar-Based Estimates of Pyrogenic O_3

The NREL AERONET measurements, HRRR-smoke, and HYSPLIT trajectories in Supporting Information S1 suggest that a major influx of smoke from the Bootleg Fire in Oregon and multiple smaller fires in Idaho reached the Denver-Boulder area on 10 and 11 July, and the TOPAZ curtain plots in Figure 15 contrast the measured O_3 and β distributions above Boulder before (8 and 9 July) and after (12 July) the arrival of this smoke. 8 July was unusually hot with a peak temperature above 40°C at the DSRC, but the 5-min surface O_3 measurements at the DSRC only very briefly reached 60 ppbv and the MDA8 plateaued at 53 ppbv because of strong westerly flow aloft. The curtain plots show that the low O_3 and β extended throughout the lower troposphere with mean values of 58.7 ± 1.3 ppbv and 0.68 ± 0.02 × 10^{-6} m^{-1} sr^{-1} within the reference region defined by the dashed box (1030–1230 MST, 2–3 km a.g.l.). 9 July was slightly cooler (T_{max} = 37°C), but the synoptic flow was weak allowing southeasterly upslope flow to develop early in the day causing a rapid buildup of O_3 and aerosol within the much deeper (≈1.7 km) convective boundary layer. The 5-min O_3 reached 105 ppbv, but the peak was followed by an equally rapid decline when the boundary layer was vented by deep convection in mid-afternoon. The MDA8 concentration still exceeded the NAAQS at 74 ppbv, however. There were no TOPAZ measurements on 10 or 11 July, but temperatures continued to moderate and the 5-min surface O_3 concentrations peaked at 78 and 83 ppbv, respectively, on these two days with the MDA8 O_3 concentrations reaching 71 and 73 ppbv. The O_3 and β in the free tropospheric reference region (56.2 ± 1.4 ppbv and 1.15 ± 0.10 × 10^{-6} m^{-1} sr^{-1}) was similar to that measured on the previous day. Similar measurements (not shown) from 24 August (52 ± 2 ppbv and 0.79 ± 0.07 × 10^{-6} m^{-1} sr^{-1}) and 16 September (53 ± 3 ppbv and 0.52 ± 0.06 × 10^{-6} m^{-1} sr^{-1}) found the free tropospheric baseline O_3 to be about 5% lower.

Figure 15c shows the initial appearance of smoke aloft and the mean O_3 and β in the reference region increased to 73.5 ± 5.7 ppbv and 12.9 ± 0.6 × 10^{-6} m^{-1} sr^{-1}, respectively. Southeasterly winds persisted throughout the day, but the peak surface concentrations were slightly lower (98 ppbv) than those on 9 July. However, there was no cloud cover or convective venting and the high O_3 persisted much longer allowing the MDA8 to reach 84 ppbv. The curtain plot clearly shows entrainment of the smoke around 2 km by the growing BL. Figure 16 shows the relationship between the backscatter and O_3 enhancements in the lower free troposphere relative to the baseline

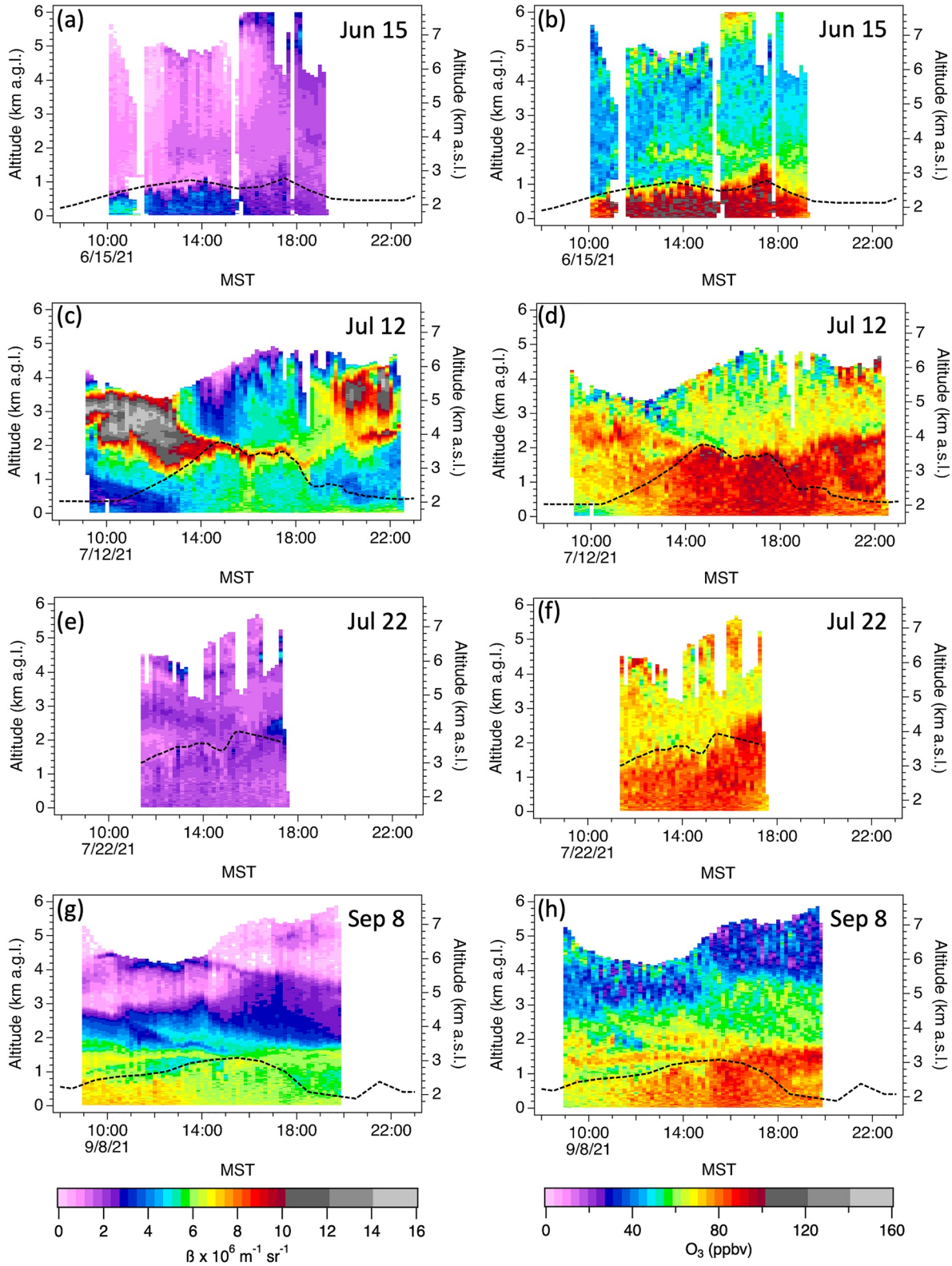

Figure 14. Time-height curtain plots of the (left) particulate backscatter (β) and (right) O_3 measured by TOPAZ on (a) 15 June, (b) 12 July, (c) 22 July, and (d) 8 September. The dashed black lines show the boundary layer heights (see text).

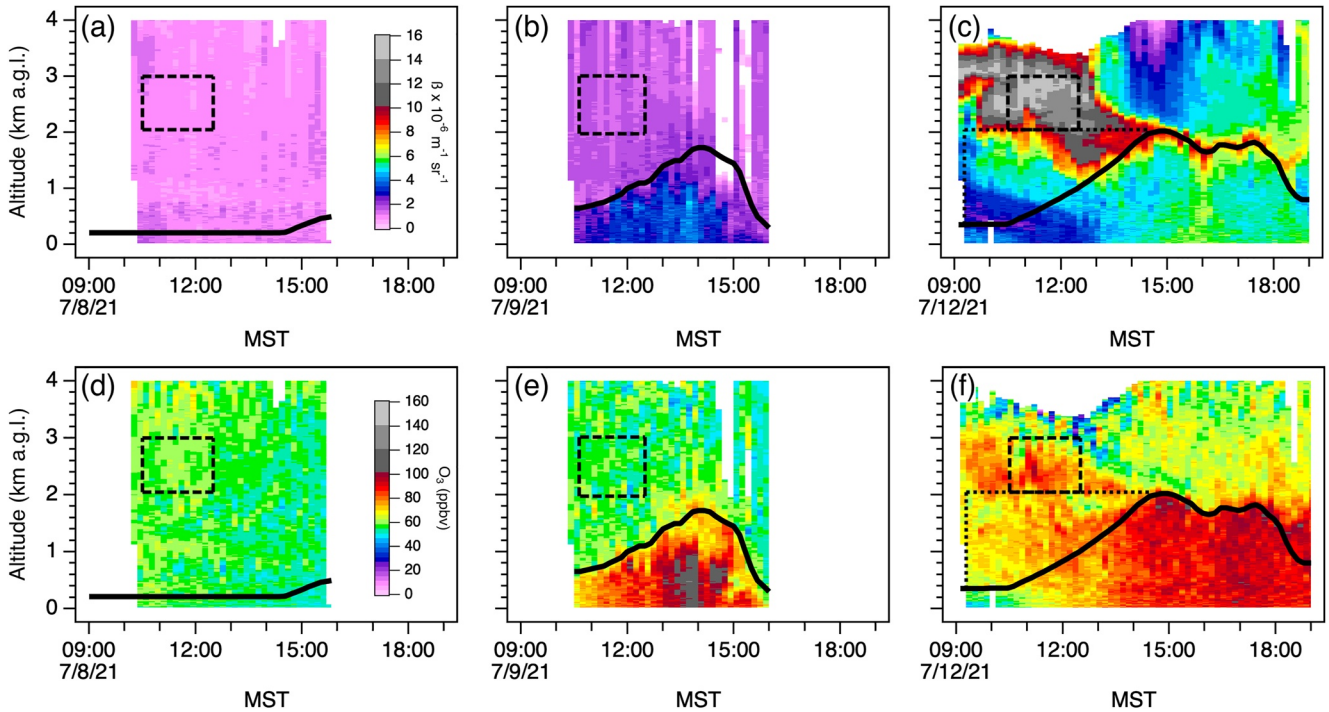

Figure 15. Backscatter (top) and O_3 (bottom) curtain plots for 8 July (left), 9 July (center), and 12 July (right). The mean O_3 mixing ratios within the dashed boxes (1030–1230 MST, 2–3 km) are 58.7 ± 1.3, 56.2 ± 1.4, and 73.5 ± 5.7 ppbv. The corresponding β values are 0.68 ± 0.02, 1.15 ± 0.10, and 12.9 ± 0.6 × 10^{-6} m^{-1} sr^{-1}. The solid lines show the boundary layer and the dotted lines in (c and f) define the regions used to estimate the smoke entrainment.

values described above. These measurements are represented by the filled triangles which show the mean O_3 and β concentrations averaged from the top of the boundary layer to 2 km a.g.l. and binned into 1-hr intervals from 0900 to 1400 MST. The filled diamonds, squares, and circles show the hourly binned measurements from 8, 9 and 12 July, respectively, averaged over the 2–3 km free tropospheric reference region with the mean baseline O_3 and β measured on 8 and 9 July subtracted. These points can be fit by an exponential curve (solid red line):

$$\Delta O_3 = (21.5 \pm 2.8)\left(1 - \exp^{-(0.245\pm0.09)\Delta\beta}\right) \quad (1)$$

The black crosses show lower free tropospheric measurements from all of the other days between 13 July and 15 September. These measurements are referenced to the same baseline values, but have different averaging times and are not used in the least-square fitting. They mostly fall within the limits of the fit uncertainties, but none of these enhancements were large enough to reach the flatter part of the curve defined by the measurements from 12 July.

Equation 1 differs from the simple linear relationships found for the TOPAZ O_3 and β measurements in smoke from the Soberanes Fire (Langford et al., 2020) during the 2016 CABOTS field study (Faloona et al., 2020) where the weak vertical mixing above the San Joaquin Valley caused the smoke aloft to remain stratified and disperse horizontally as it recirculated around the valley. The ozone enhancement in the Soberanes smoke ranged from $\Delta O_3/\Delta\beta \approx 12 \times 10^6$ ppbv m sr for the diffuse smoke haze to $\approx 3 \times 10^6$ ppbv m sr in the denser plumes and Figure 16 shows that the measurements from the densest part of the smoke plume in Figure 15c correspond to a $\Delta O_3/\Delta\beta$ ratio of $\approx 2 \times 10^6$ ppbv m sr. These lower values are attributed to a combination of reduced actinic flux and gaseous losses to the smoke particles in the denser plumes (Buysse et al., 2019).

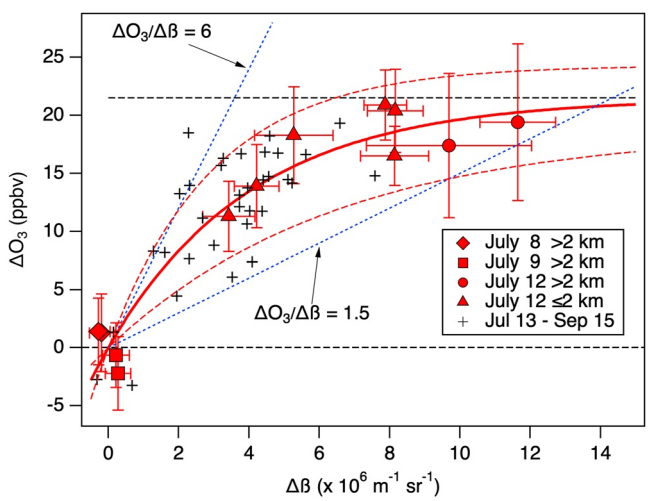

Figure 16. Scatter plot comparing the hourly binned and vertically averaged O_3 and β measurements from the 2–3 km dashed boxes in Figure 15, and the region between the top of the boundary layer and 2 km a.g.l. on Jul 12. The error bars show the standard deviations of the averages. The solid red curve shows the least squares fit of these data to Equation 1 with the fit uncertainties represented by the dashed red curves. The "+" symbols show lower free tropospheric samples from other days between 13 July and 15 September. The O_3 enhancement in the main part of the smoke plume is ≈22 ppbv. The dotted blue lines bracket the measurements with linear relationships corresponding to $\Delta O_3/\Delta\beta = 1.5$ and 6×10^6 ppbv m sr.

5.2. Entrainment of Smoke and O_3 Into the Boundary Layer

We can estimate the contribution of entrained pyrogenic O_3 to the total observed O_3 burden in the BL on 12 July using the relationship in Equation 1 together with the budget equation for pyrogenic O_3 within the BL ($O_{3\,\text{fire BL}}$)

$$\frac{\partial O_{3\,\text{fire BL}}}{\partial t} + u\frac{\partial O_{3\,\text{fire BL}}}{\partial x} = -\frac{\partial \overline{w'O'_{3\,\text{fire BL}}}}{\partial z} + S_{O3\,\text{fire BL}} \tag{2}$$

Here, the local time rate of change and horizontal advection terms on the left side are balanced by the vertical turbulent flux gradient and source/sink terms ($S_{O3\,\text{fire BL}}$) on the right side. The budget terms for the non-pyrogenic portion of BL O_3 do not need to be considered here because we are attempting to quantify only the pyrogenic portion and not the entire O_3 burden in the BL. The horizontal advection term can be neglected on 12 July since smoke was not yet widespread along the Front Range, but some buildup of photochemically generated particles would have been present even in the absence of smoke (cf. Figure 15b). The regional photochemistry would also have generated significant O_3 (cf. Figure 15e), but we neglect the photochemical production of O_3 from co-entrained wildfire VOCs reacting with urban NO_x as discussed in Section 4. That leaves the vertical turbulent flux gradient across the BL, which is driven by the entrainment flux, as the dominant $O_{3\,\text{fire BL}}$ budget term and Equation 2 reduces to:

$$\frac{\partial O_{3\,\text{fire BL}}}{\partial t} = -\frac{\overline{w'O'_{3\,\text{fire BL}z_i}} - \overline{w'O'_{3\,\text{fire BL}0}}}{z_i} = \frac{w_e(O_{3\,\text{fire LFT}} - O_{3\,\text{fire BL}}) - v_D O_{3\,\text{fire BL}}}{z_i} \tag{3}$$

We do not have access to direct eddy correlation O_3 flux observation. Therefore, as is customary, we parameterize the O_3 entrainment flux as the product of entrainment velocity w_e and the O_3 concentration difference across the BL–LFT interface. Similarly, we represent the O_3 surface flux as the product of deposition velocity v_D and BL O_3 concentration. The entrainment velocity can be written as:

$$w_e = \frac{\partial z_i}{\partial t} + u\frac{\partial z_i}{\partial x} - w_L \tag{4}$$

with z_i representing the mixed layer height and w_L the large-scale vertical velocity. Because of a lack of spatially distributed zi observations and given the generally low horizontal wind speeds, we neglect the mixed layer height advection term in Equation 4. The large-scale vertical velocity is typically very small (on the order of mm s^{-1}) and is essentially impossible to measure accurately and difficult to model correctly. Therefore, we omit w_L in Equation 4. We also set the deposition velocity and thus the surface pyrogenic O_3 flux to zero. v_D tends to be small, but is highly variable and dependent on surface land cover and near-surface turbulence characteristics. Neglecting deposition causes an overestimation of the wild fire O_3 time rate of change, whereas omission of w_L (which should be slightly negative under high pressure synoptic conditions) leads to an underestimation of w_e, entrainment flux, and, in turn O_3 time rate of change. Both errors are estimated to be in the 10%–30% range, but have opposite signs, leading to a smaller combined error. With the above assumptions the wildfire BL O_3 budget equation reduces to:

$$\frac{\partial O_{3\,\text{fire BL}}}{\partial t} = \frac{\frac{\partial z_i}{\partial t}(O_{3\,\text{fire LFT}} - O_{3\,\text{fire BL}})}{z_i} \tag{5}$$

This differential equation can easily be solved for $O_{3\,\text{fire BL}}$. We determined $O_{3\,\text{fire LFT}}$ by first averaging TOPAZ $\Delta\beta$ data vertically over 50 m just above the entrainment zone and then converted $\Delta\beta$ to LFT fire O_3 using Equation 1. Following Deardorff et al. (1980), we assumed an entrainment zone symmetric around z_i with a thickness of 0.2 z_i. Thus, we averaged the TOPAZ $\Delta\beta$ data between 1.1 × z_i and 1.1 × z_i + 50 m. z_i and its time derivative were determined from the vertical velocity variance data from the collocated Doppler lidar. The hourly z_i and $\partial z_i/\partial t$ data were interpolated onto the 10-min TOPAZ time grid. If either $\Delta\beta$ or $\partial z_i/\partial t$ were negative they were set to zero. Assuming that there is no fire O_3 in the BL at the beginning of the daily TOPAZ observations, Equation 5 readily yields a time series of BL fire O_3 at each TOPAZ 10-min time step. The $O_{3\,\text{fire BL}}$ data were averaged onto a 1-hr grid and then further averaged using a moving 8-hr window. If 8 hr of consecutive hourly data were not available, the boxcar window was reduced to no less than 6 hr, consistent with the EPA method to determine O_3 MDA8. The MDA8 wildfire contribution was chosen as the "8-hr" wildfire BL O_3 value for the same hour when MDA8 O_3 at the Rocky Flats site was reached. Our calculations suggest that entrained wildfire smoke increased

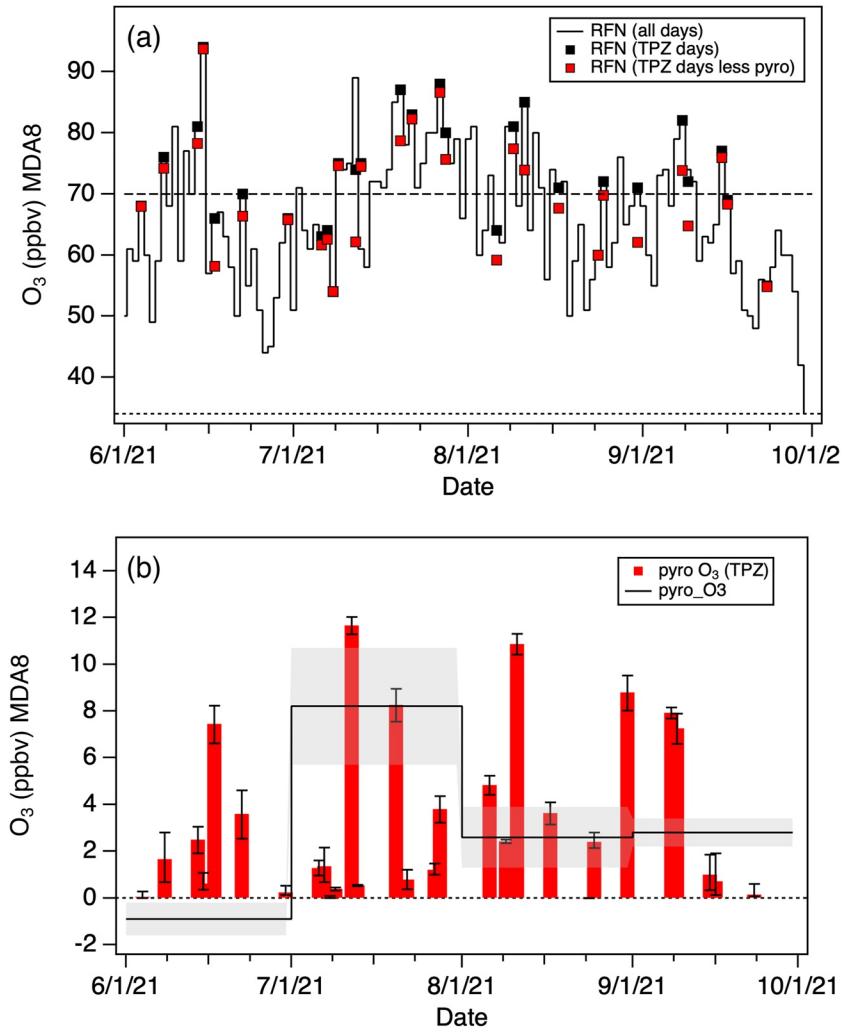

Figure 17. (a) MDA8 O_3 measured by the Rocky Flats (RFN) monitor (staircase). The black squares mark the 29 days with TOPAZ lidar measurements. The red squares show the MDA8 measurements with the pyrogenic O_3 contribution derived from the lidar measurements subtracted. (b) Pyrogenic O_3 contributions estimated from the lidar measurements (red bars). The staircase shows the monthly mean contributions (with standard deviations in gray estimated from the regulatory measurements.

the MDA8 concentrations in the Boulder/Rocky Flats area by ≈ 12 ± 1 ppbv on 12 July, with the error bar determined primarily by the uncertainties in Equation 1 and an estimated uncertainty of ±30% in the assumed baseline for β and to a lesser extent the assumed entrainment zone thickness (z_i) (Deardorff, 1980).

Estimates of the pyrogenic O_3 contribution to the MDA8 on the 29 days with enough TOPAZ measurements are plotted in Figure 17 along with the MDA8 O_3 measurements from Rocky Flats. The contributions for the days following 12 July are more uncertain and should be considered upper limits since horizontal advection of smoke that was entrained previously, but has been depleted in O_3 by surface deposition could have occurred. The next largest influx after 12 July was on 11 August (≈11 ppbv) several days after the large smoke incursion of 7 and 8 August. The estimated wildfire contribution on 8 September was ≈8 ppbv, but the estimates for 15 June and 22 July, the other two peak O_3 days, are only ≈0.6 and 0.8 ppbv, respectively. The mean contribution on all 29 days was 3.3 ppbv, which is comparable to the value inferred from the surface measurements for the 122 days from 1 June to 30 September in Section 4.

6. Implications for NAAQS Attainment

The monthly mean MDA8 O_3 concentrations measured by the Rocky Flats (Figure 10d) and Chatfield (Figure 10f) monitors in July of 2021 were 72.0 and 77.0 ppbv, respectively. The Chatfield monitor exceeded the 2015 NAAQS

on 17 days in July, and 4 of the 8 days with missing data would probably have also been in exceedance for a total of 21. Of the 17 days that did have measurements, 12 would have still exceeded the NAAQS if the MDA8 was reduced by the average pyrogenic O_3 contribution of 8 ppbv. There were no data gaps at the nearby Highland Reservoir and NREL monitors (cf. Figure 1b), and these two monitors exceeded the NAAQS on 22 and 20 days, respectively. The corresponding numbers would have been 13 and 16 without the pyrogenic O_3. The RFN monitor also exceeded the 2015 NAAQS on 21 of the 31 days in July, but would only have exceeded on 10 days without the pyrogenic O_3. These differences could reflect the additional contributions from the reactions of PVOCs at the three monitors on the southwest side of Denver.

The TOPAZ lidar was usually operated on days when high O_3 was anticipated and the 29 days with measurements include 18 of the 47 days when the 2015 NAAQS was exceeded. The mean MDA8 O_3 measured by the Rocky Flats monitor on these days was 73.2 ± 9.8 ppbv or about 7 ppbv higher than the mean of 66.1 ± 11.1 for all 122 days (cf. Table 2). The mean MDA8 would decrease to 69.9 ± 9.5 ppbv without the estimated pyrogenic O_3 contributions, and 5 of the 18 exceedances days in Figure 17a would fall below the NAAQS.

7. Summary and Conclusions

We have used two independent methods to estimate the contributions of pyrogenic O_3 to the surface concentrations in northern Colorado during the summer of 2021, and examined the impact of this transport on NAAQS exceedances in the Denver metro/Northern Front Range (DM/NFR) nonattainment area. In the first method, we compare surface O_3 and $PM_{2.5}$ measurements from the DM/NFR with those from the sparsely populated Western Slope (WSLP) where photochemical production of O_3 is minimal. In the second method, we use lidar measurements from Boulder to estimate the direct entrainment of O_3-enriched smoke from the lower free troposphere into the boundary layer. Both approaches suggest that pyrogenic O_3 increased the mean MDA8 O_3 concentrations by an average of ≈3 ppbv between 1 June and 30 September 2021 although the 2–3 times per week sampling increases the uncertainty in the lidar-based estimate. The largest wildfire influence was in July when pyrogenic O_3 appears to have increased the MDA8 concentrations across the entire northern half of the state by an average of about 8 ppbv, although the lidar measurements show that there was much day-to-day variability in the actual amounts. The estimated monthly mean contributions for June, August, and September were much smaller (0–3 ppbv). Most model-based studies do not separate the transport and photochemical contributions, but these numbers are comparable to the 5–9 ppbv estimated for the pyrogenic O_3 transported to the Western U.S. in Siberian wildfire smoke (Jaffe et al., 2004), and the 4.3 ppbv derived by analyzing measurements from "smoke" and "non smoke" days in Denver (2008–2015) with a generalized additive model (GAM) (Gong et al., 2017).

The available measurements do not allow us to fully decouple the spatially variable O_3 enhancements caused by reactions of PVOCs with anthropogenic NO_x from the enhancements caused by the unusual meteorology in 2021 (i.e., clearer skies, warmer temperatures, weaker winds, and fewer thunderstorms). Our analysis suggests that their combined contributions were 3 ppbv or less in the Boulder area, which was previously shown to be NO_x sensitive (Rickly et al., 2023), and up to 12 ppbv in the suburbs south and west of downtown Denver where more NO_x was generally available.

Data Availability Statement

The surface measurements used in our analyses were downloaded from the U.S. EPA Air Quality System (AQS) (https://aqs.epa.gov/aqsweb/airdata/download_files.html#Daily) and the TOPAZ lidar data are archived at https://www-air.larc.nasa.gov/missions/TOLNet/data.html. The Denver International Airport (DIA) weather observations were downloaded from the local NWS website (https://www.weather.gov/bou/). The Vaisala National Lightning Detection Network (NLDN) data were obtained from the NOAA National Center for Environmental Information (NCEI, DSI 9603_02 gov.noaa.ncdc:C00989) and the Boulder Airport winds from the NCEI Integrated Surface Database (https://www.ncei.noaa.gov/products/land-based-station/integrated-surface-database). The MesoWest data were downloaded from (https://mesowest.utah.edu) and the AERONET data from (https://aeronet.gsfc.nasa.gov/new_web/data.html). The National Centers for Environmental Prediction/National Center for Atmospheric Research (NCEP/NCAR) Re-analysis and National Centers for Environmental Prediction (NCEP) North American Regional Re-analysis (NARR) images were plotted using the online tools provided by the NOAA Physical Sciences Laboratory, Boulder Colorado on their website at https://psl.noaa.gov/.

Acknowledgments
The NOAA CSL lidar operations were supported by the NOAA Climate Program Office, Atmospheric Chemistry, Carbon Cycle, and Climate (AC4) Program and the NASA-sponsored Tropospheric Ozone Lidar Network (TOLNet, http://www-air.larc.nasa.gov/missions/TOLNet/). This work was supported in part by the NOAA Cooperative Agreement with CIRES, NA17OAR4320101. We would like to thank Scott Landes, Dan Welsh, and Erick Mattson of the Colorado Department of Public Health and the Environment for help with the monitoring data. We would also like to thank Brent Holben, and the rest of the AERONET staff for maintaining the network and making the AERONET data available. The views, opinions, and findings contained in this report are those of the author(s) and should not be construed as an official National Oceanic and Atmospheric Administration or U.S. Government position, policy, or decision.

References

Ahmadov, R., Grell, G., James, E., Csiszar, I., Tsidulko, M., Pierce, R. B., et al. (2017). Using VIIRS fire radiative power data to simulate biomass burning emissions, plume rise and smoke transport in a real-time air quality modeling system. *Paper presented at International Journal of Geoscience and Remote Sensing* (pp. 23–28).

Alvarado, M. J., Logan, J. A., Mao, J., Apel, E., Riemer, D., Blake, D., et al. (2010). Nitrogen oxides and PAN in plumes from boreal fires during ARCTAS-B and their impact on ozone: An integrated analysis of aircraft and satellite observations. *Atmospheric Chemistry and Physics*, *10*(20), 9739–9760. https://doi.org/10.5194/Acp-10-9739-2010

Alvarez, R. J., Senff, C. J., Langford, A. O., Weickmann, A. M., Law, D. C., Machol, J. L., et al. (2011). Development and application of a compact, tunable, solid-state airborne ozone lidar system for boundary layer profiling. *Journal of Atmospheric and Oceanic Technology*, *28*(10), 1258–1272. https://doi.org/10.1175/Jtech-D-10-05044.1

Bartusek, S., Kornhuber, K., & Ting, M. (2022). 2021 North American heatwave amplified by climate change-driven nonlinear interactions. *Nature Climate Change*. https://doi.org/10.1038/s41558-022-01520-4

Bonin, T. A., Carroll, B. J., Hardesty, R. M., Brewer, W. A., Hajny, K., Salmon, O. E., & Shepson, P. B. (2018). Doppler lidar observations of the mixing height in Indianapolis using an automated composite fuzzy Logic approach. *Journal of Atmospheric and Oceanic Technology*, *35*(3), 473–490. https://doi.org/10.1175/Jtech-D-17-0159.1

Bourgeois, I., Peischl, J., Neuman, J. A., Brown, S. S., Thompson, C. R., Aikin, K. C., et al. (2021). Large contribution of biomass burning emissions to ozone throughout the global remote troposphere. *Proceedings of the National Academy of Sciences of the United States of America*, *118*(52), e2109628118. https://doi.org/10.1073/pnas.2109628118

Brown, J. S., Bateson, T. F., & McDonnell, W. F. (2008). Effects of exposure to 0.06 ppm ozone on FEV1 in humans: A secondary analysis of existing data. *Environmental Health Perspectives*, *116*(8), 1023–1026. https://doi.org/10.1289/ehp.11396

Bryant, B. P., & Westerling, A. L. (2014). Scenarios for future wildfire risk in California: Links between changing demography, land use, climate, and wildfire. *Environmetrics*, *25*(6), 454–471. https://doi.org/10.1002/env.2280

Buysse, C. E., Kaulfus, A., Nair, U., & Jaffe, D. A. (2019). Relationships between particulate matter, ozone, and nitrogen oxides during urban smoke events in the Western US. *Environmental Science & Technology*, *53*(21), 12519–12528. https://doi.org/10.1021/acs.est.9b05241

Calahorrano, J. F. J., Lindaas, J., O'Dell, K., Palm, B. B., Peng, Q., Flocke, F., et al. (2021). Daytime oxidized reactive nitrogen partitioning in Western US wildfire smoke plumes. *Journal of Geophysical Research: Atmosphere*, *126*(4), e2020JD033484. https://doi.org/10.1029/2020jd033484

Chen, G., Xue, H., Feingold, G., & Zhou, X. (2012). Vertical transport of pollutants by shallow cumuli from large eddy simulations. *Atmospheric Chemistry and Physics*, *12*(23), 11319–11327. https://doi.org/10.5194/acp-12-11319-2012

Choukulkar, A., Brewer, W. A., Sandberg, S. P., Weickmann, A., Bonin, T. A., Hardesty, R. M., et al. (2017). Evaluation of single and multiple Doppler lidar techniques to measure complex flow during the XPIA field campaign. *Atmospheric Measurement Techniques*, *10*(1), 247–264. https://doi.org/10.5194/amt-10-247-2017

Cotton, W. R., Alexander, G. D., Hertenstein, R., McAnelly, R. L., Walko, R. L., & Nicholls, M. (1995). Cloud venting -A review and some new global annual estimates. *Earth-Science Reviews*, *39*(3–4), 169–206. https://doi.org/10.1016/0012-8252(95)00007-0

Deardorff, J. W., Willis, G. E., & Stockton, B. H. (1980). Laboratory studies of the entrainment zone of a convectively mixed layer. *Journal of Fluid Mechanics*, *100*(1), 41–64. https://doi.org/10.1017/S0022112080001000

Dreessen, J., Sullivan, J., & Delgado, R. (2016). Observations and impacts of transported Canadian wildfire smoke on ozone and aerosol air quality in the Maryland region on June 9-12, 2015. *Journal of the Air and Waste Management Association*, *66*(9), 842–862. https://doi.org/10.1080/10962247.2016.1161674

Environment and Climate Change Canada (2021). Adapting to the impacts of climate change in Canada: An update on the National Adaptation Strategy. Rep. En4-473/2021E-PDF.

Faloona, I. C., Chiao, S., Eiserloh, A. J., Alvarez, R. J., Kirgis, G., Langford, A. O., et al. (2020). The California baseline ozone transport study (CABOTS). *Bulletin of the American Meteorological Society*, *101*(4), E427–E445. https://doi.org/10.1175/Bams-D-18-0302.1

Fehsenfeld, F. C., Bollinger, M. J., Liu, S. C., Parrish, D. D., McFarland, M., Trainer, M., et al. (1983). A study of ozone in the Colorado mountains. *Journal of Atmospheric Chemistry*, *1*, 87–105. https://doi.org/10.1007/bf00113981

Flocke, F., Pfister, G., Crawford, J. H., Pickering, K. E., Pierce, G., Bon, D., & Reddy, P. (2020). Air quality in the northern Colorado front range metro area: The front range air pollution and photochemistry experiment (FRAPPE). *Journal of Geophysical Research: Atmosphere*, *125*(2), e2019JD031197. https://doi.org/10.1029/2019JD031197

Gaudel, A., Cooper, O. R., Ancellet, G., Barret, B., Boynard, A., Burrows, J. P., et al. (2018). Tropospheric Ozone Assessment Report: Present-day distribution and trends of tropospheric ozone relevant to climate and global atmospheric chemistry model evaluation. *Elementa: Science of the Anthropocene*, *6*, 39. https://doi.org/10.1525/elementa.291

Gong, X., Kaulfus, A., Nair, U., & Jaffe, D. A. (2017). Quantifying O-3 impacts in urban areas due to wildfires using a generalized additive model. *Environmental Science & Technology*, *51*(22), 13216–13223. https://doi.org/10.1021/acs.est.7b03130

Jaffe, D. A., Bertschi, I., Jaeglé, L., Novelli, P., Reid, J. S., Tanimoto, H., et al. (2004). Long-range transport of Siberian biomass burning emissions and impact on surface ozone in Western North America. *Geophysical Research Letters*, *31*(16), L16106. https://doi.org/10.1029/2004gl020093

Jaffe, D. A., Cooper, O. R., Fiore, A. M., Henderson, B. H., Tonneson, G. S., Russell, A. G., et al. (2018). Scientific assessment of background ozone over the U.S.: Implications for air quality management. *Elementa: Science of the Anthropocene*, *6*(1). https://doi.org/10.1525/elementa.309

Jaffe, D. A., & Wigder, N. L. (2012). Ozone production from wildfires: A critical review. *Atmospheric Environment*, *51*, 1–10. https://doi.org/10.1016/J.Atmosenv.2011.11.063

Jiang, J. H., Su, H., Huang, L., Wang, Y., Massie, S., Zhao, B., et al. (2018). Contrasting effects on deep convective clouds by different types of aerosols. *Nature Communications*, *9*(1), 3874. https://doi.org/10.1038/s41467-018-06280-4

Johnson, M. S., Strawbridge, K., Knowland, K. E., Keller, C., & Travis, M. (2021). Long-range transport of Siberian biomass burning emissions to North America during FIREX-AQ. *Atmospheric Environment*, *252*, 118241. https://doi.org/10.1016/j.atmosenv.2021.118241

Kalashnikov, D. A., Schnell, J. L., Abatzoglou, J. T., Swain, D. L., & Singh, D. (2022). Increasing co-occurrence of fine particulate matter and ground-level ozone extremes in the Western United States. *Science Advances*, *8*(1), eabi9386. https://doi.org/10.1126/sciadv.abi9386

Karstadt, M., Callaghan, B., & United States Environmental Protection Agency Office of Air and Radiation. (1993). *The plain English guide to the Clean Air Act*, (p. 28). U.S. Environmental Protection Agency For sale by the U.S. G.P.O., Supt. of Docs., Washington, DC.

Kuang, S., Newchurch, M. J., Johnson, M. S., Wang, L., Burris, J., Pierce, R. B., et al. (2017). Summertime tropospheric ozone enhancement associated with a cold front passage due to stratosphere-to-troposphere transport and biomass burning: Simultaneous ground-based lidar and airborne measurements. *Journal of Geophysical Research: Atmosphere*, *122*(2), 1293–1311. https://doi.org/10.1002/2016jd026078

Langford, A. O., Alvarez, R. J., Brioude, J., Caputi, D., Conley, S. A., Evan, S., et al. (2020). Ozone production in the Soberanes smoke haze: Implications for air quality in the San Joaquin Valley during the California baseline ozone transport study. *Journal of Geophysical Research: Atmosphere*, *125*(11), e2019JD031777. https://doi.org/10.1029/2019JD031777

Langford, A. O., Alvarez II, R. J., Kirgis, G., Senff, C. J., Caputi, D., Conley, S. A., et al. (2019). Intercomparison of lidar, aircraft, and surface ozone measurements in the San Joaquin Valley during the California baseline ozone transport study (CABOTS). *Atmospheric Measurement Techniques*, *12*(3), 1889–1904. https://doi.org/10.5194/amt-12-1889-2019

Langford, A. O., Tucker, S. C., Senff, C. J., Banta, R. M., Brewer, W. A., Alvarez, R. J., et al. (2010). Convective venting and surface ozone in Houston during TexAQS 2006. *Journal of Geophysical Research*, *115*(D16), D16305. https://doi.org/10.1029/2009jd013301

Lin, C. A., Lu, C. H., Chen, S. P., Hung, W. T., Civerolo, K. L., & Rattigan, O. V. (2021). Characterization of intra-continental smoke transport and impact on New York State air quality using aerosol reanalysis and multi-platform observations. *Atmospheric Pollution Research*, *12*(3), 154–166. https://doi.org/10.1016/j.apr.2021.01.021

McDuffie, E. E., Edwards, P. M., Gilman, J. B., Lerner, B. M., Dubé, W. P., Trainer, M., et al. (2016). Influence of oil and gas emissions on summertime ozone in the Colorado Northern Front Range. *Journal of Geophysical Research: Atmosphere*, *121*(14), 8712–8729. https://doi.org/10.1002/2016jd025265

McKeen, S. A., Wotawa, G., Parrish, D. D., Holloway, J. S., Buhr, M. P., Hübler, G., et al. (2002). Ozone production from Canadian wildfires during June and July of 1995. *Journal of Geophysical Research*, *107*(D14), 4192. https://doi.org/10.1029/2001JD000697

National Weather Service. (2023). WFO monthly/daily climate data. Retrieved from https://forecast.weather.gov/product.php?site=BOU&product=CF6&issuedby=DEN

Nikonovas, T., North, P. R. J., & Doerr, S. H. (2015). Smoke aerosol properties and ageing effects for northern temperate and boreal regions derived from AERONET source and age attribution. *Atmospheric Chemistry and Physics*, *15*(14), 7929–7943. https://doi.org/10.5194/acp-15-7929-2015

Ninneman, M., & Jaffe, D. A. (2021). The impact of wildfire smoke on ozone production in an urban area: Insights from field observations and photochemical box modeling. *Atmospheric Environment*, *267*, 118764. https://doi.org/10.1016/j.atmosenv.2021.118764

NOAA National Centers for Environmental Information. (2022). Washington maximum temperature. Retrieved from https://www.ncei.noaa.gov/monitoring-content/extremes/scec/reports/20220210-Washington-Maximum-Temperature.pdf

Pachon, J. E., Weber, R. J., Zhang, X. L., Mulholland, J. A., & Russell, A. G. (2013). Revising the use of potassium (K) in the source apportionment of PM2.5. *Atmospheric Pollution Research*, *4*(1), 14–21. https://doi.org/10.5094/Apr.2013.002

Pollack, I. B., Helmig, D., O'Dell, K., & Fischer, E. V. (2021). Weekend-weekday implications and the impact of wildfire smoke on ozone and its precursors at Boulder Reservoir, Colorado between 2017 and 2019. *Journal of Geophysical Research: Atmosphere*, *126*(17), e2021JD035221. https://doi.org/10.1029/2021JD035221

Reddy, P. J., & Pfister, G. G. (2016). Meteorological factors contributing to the interannual variability of midsummer surface ozone in Colorado, Utah, and other Western US states. *Journal of Geophysical Research: Atmosphere*, *121*(5), 2434–2456. https://doi.org/10.1002/2015jd023840

Reid, C. E., Brauer, M., Johnston, F. H., Jerrett, M., Balmes, J. R., & Elliott, C. T. (2016). Critical review of health impacts of wildfire smoke exposure. *Environmental Health Perspectives*, *124*(9), 1334–1343. https://doi.org/10.1289/ehp.1409277

Rickly, P. S., Coggon, M. M., Aikin, K. C., Alvarez, R. J., Baidar, S., Gilman, J. B., et al. (2023). Influence of wildfire on urban ozone: An observationally constrained box modeling study at a site in the Colorado front range. *Environmental Science & Technology*, *57*(3), 1257–1267. https://doi.org/10.1021/acs.est.2c06157

Robinson, M. A., Decker, Z. C. J., Barsanti, K. C., Coggon, M. M., Flocke, F. M., Franchin, A., et al. (2021). Variability and time of day dependence of ozone photochemistry in Western wildfire plumes. *Environmental Science & Technology*, *55*(15), 10280–10290. https://doi.org/10.1021/acs.est.1c01963

Schaaf, C. B., Wurman, J., & Banta, R. M. (1988). Thunderstorm-producing terrain features. *Bulletin of the American Meteorological Society*, *69*(3), 272–277. https://doi.org/10.1175/1520-0477(1988)069<0272:tptf>2.0.co;2

Scheffe, R. D., Solomon, P. A., Husar, R., Hanley, T., Schmidt, M., Koerber, M., et al. (2009). The National ambient air monitoring strategy: Rethinking the role of National networks. *Journal of the Air and Waste Management Association*, *59*(5), 579–590. https://doi.org/10.3155/1047-3289.59.5.579

Sillman, S., & Samson, P. J. (1995). Impact of temperature on oxidant photochemistry in urban, polluted rural and remote environments. *Journal of Geophysical Research*, *100*(D6), 12. https://doi.org/10.1029/94jd02146

Singh, H. B., Cai, C., Kaduwela, A., Weinheimer, A., & Wisthaler, A. (2012). Interactions of fire emissions and urban pollution over California: Ozone formation and air quality simulations. *Atmospheric Environment*, *56*, 45–51. https://doi.org/10.1016/J.Atmosenv.2012.03.046

State of Colorado. (2023). *State demography Office*. SDO State and Regional Data Resource Page. Retrieved from https://demography.dola.colorado.gov/assets/html/state.html

Stein, A. F., Draxler, R. R., Rolph, G. D., Stunder, B. J. B., Cohen, M. D., & Ngan, F. (2015). NOAA'S HYSPLIT atmospheric transport and dispersion modeling system. *Bulletin America Meteorology Social*, *96*(12), 2059–2077. https://doi.org/10.1175/Bams-D-14-00110.1

Sullivan, J. T., McGee, T. J., Langford, A. O., Alvarez, R. J., Senff, C. J., Reddy, P. J., et al. (2016). Quantifying the contribution of thermally driven recirculation to a high-ozone event along the Colorado Front Range using lidar. *Journal of Geophysical Research: Atmosphere*, *121*(17), 10377–10390. https://doi.org/10.1002/2016jd025229

Thompson, V., Kennedy-Asser, A. T., Vosper, E., Lo, Y. T. E., Huntingford, C., Andrews, O., et al. (2022). The 2021 Western North America heat wave among the most extreme events ever recorded globally. *Science Advances*, *8*(18), eabm6860. https://doi.org/10.1126/sciadv.abm6860

US Environmental Protection Agency. (2022a). *Determinations of attainment by the attainment date, extensions of the date, attainment date, and reclassification of areas classified as marginal for the 2015 ozone National ambient air quality standards, quality standards, in EPA–HQ–OAR–2021–0742; FRL–8425–02–OAR*. U. S. Environmental Protection Agency, Federal Register.

US Environmental Protection Agency. (2022b). Ozone NAAQS timelines. Retrieved from https://www.epa.gov/ground-level-ozone-pollution/ozone-naaqs-timelines

US Environmental Protection Agency. (2022c). *Determinations of attainment by the attainment date, extensions of the attainment date, and reclassification of areas classified as serious for the 2008 ozone National ambient air quality standards, in EPA–HQ–OAR–2021–0741; FRL–8426–02–OAR*. U. S. Environmental Protection Agency, Federal Register.

US Environmental Protection Agency. (2023a). Air quality system data Mart. [internet database] available via Retrieved from https://www.epa.gov/outdoor-air-quality-data

US Environmental Protection Agency. (2023b). *Nonattainment areas for criteria pollutants*. Green Book). Retrieved from https://www.epa.gov/green-book

Wang, B., Kuang, S., Pfister, G. G., Pour-Biazar, A., Buchholz, R. R., Langford, A. O., & Newchurch, M. J. (2021). Impact of the 2016 southeastern US wildfires on the vertical distribution of ozone and aerosol at Huntsville, Alabama. *Journal of Geophysical Research: Atmosphere*, *126*(9). https://doi.org/10.1029/2021JD034796

Westerling, A. L., Brown, T. J., Schoennagel, T., Swetnam, T. W., Turner, M. G., & Veblen, T. T. (2016). Climate and wildfire in Western US forests. *Forest Conservation in the Anthropocene: Science, Policy, and Practice*, 43–55. https://doi.org/10.5876/9781607324591.c003

Wotawa, G., & Trainer, M. (2000). The influence of Canadian forest fires on pollutant concentrations in the United States. *Science*, *288*(5464), 5–328. https://doi.org/10.1126/science.288.5464.324

Xu, L., Crounse, J. D., Vasquez, K. T., Allen, H., Wennberg, P. O., Bourgeois, I., et al. (2021). Ozone chemistry in Western US wildfire plumes. *Science Advances*, *7*(50), eabl3648. https://doi.org/10.1126/sciadv.abl3648

References From the Supporting Information

Langford, A. O., Senff, C. J., Alvarez II, R. J., Aikin, K. C., Baidar, S., Bonin, T. A., et al. (2022). The Fires, Asian, and Stratospheric Transport–Las Vegas Ozone Study (FAST-LVOS). *Atmospheric Chemistry and Physics*, *22*(3), 1707–1737. https://doi.org/10.5194/acp-22-1707-2022

Leblanc, T., Brewer, M. A., Wang, P. S., Granados-Muñoz, M. J., Strawbridge, K. B., Travis, M., et al. (2018). Validation of the TOLNet lidars: The Southern California Ozone Observation Project (SCOOP). *Atmospheric Measurement Techniques*, *11*(11), 6137–6162. https://doi.org/10.5194/amt-11-6137-2018

Lei, L. Q., Berkoff, T. A., Gronoff, G., Su, J., Nehrir, A. R., Wu, Y. H., et al. (2022). Retrieval of UVB aerosol extinction profiles from the ground-based Langley Mobile Ozone Lidar (LMOL) system. *Atmospheric Measurement Techniques*, *15*(8), 2465–2478. https://doi.org/10.5194/amt-15-2465-2022

Muller, D., Ansmann, A., Mattis, I., Tesche, M., Wandinger, U., Althausen, D., & Pisani, G. (2007). Aerosol-type-dependent lidar ratios observed with Raman lidar. *Journal of Geophysical Research*, *112*(D16), D16202. https://doi.org/10.1029/2006jd008292

Wandinger, U., Müller, D., Böckmann, C., Althausen, D., Matthias, V., Bösenberg, J., et al. (2002). Optical and microphysical characterization of biomass burning and industrial-pollution aerosols from multi-wavelength lidar and aircraft measurements. *Journal of Geophysical Research*, *107*(D21), 21. https://doi.org/10.1029/2000jd000202

Yokelson, R. J., Burling, I. R., Urbanski, S. P., Atlas, E. L., Adachi, K., Buseck, P. R., et al. (2011). Trace gas and particle emissions from open biomass burning in Mexico. *Atmospheric Chemistry and Physics*, *11*(14), 6787–6808. https://doi.org/10.5194/acp-11-6787-2011